Available online at www.sciencedirect.com

ScienceDirect

Geochimica et Cosmochimica Acta 198 (2017) 419–438

Geochimica et Cosmochimica Acta

www.elsevier.com/locate/gca

Methane in shallow subsurface sediments at the landward limit of the gas hydrate stability zone offshore western Svalbard

Carolyn A. Graves [a,*], Rachael H. James [a], Célia Julia Sapart [b,c], Andrew W. Stott [d], Ian C. Wright [e,f], Christian Berndt [g], Graham K. Westbrook [a,h], Douglas P. Connelly [e]

[a] *Ocean and Earth Science, National Oceanography Centre, Southampton, University of Southampton, University of Southampton Waterfront Campus, Southampton SO14 3ZH, UK*

[b] *Institute for Marine and Atmospheric Research Utrecht, University of Utrecht, 3584CC Utrecht, The Netherlands*

[c] *Laboratoire de Glaciologie, Université Libre de Bruxelles, B-1050 Bruxelles, Belgium*

[d] *Natural Environment Research Council Life Sciences Mass Spectrometry Facility, Centre for Ecology and Hydrology, Lancaster LA1 4AP, UK*

[e] *National Oceanography Centre, University of Southampton Waterfront Campus, Southampton SO14 3ZH, UK*

[f] *Vice-Chancellor's Office, University of Canterbury, Christchurch 8140, New Zealand*

[g] *GEOMAR Helmholtz Centre for Ocean Research Kiel, 24148 Kiel, Germany*

[h] *Géosciences Marines, Ifremer, Brest, 29280 Plouzané, France*

Received 6 December 2015; accepted in revised form 2 November 2016; Available online 19 November 2016

Abstract

Offshore western Svalbard plumes of gas bubbles rise from the seafloor at the landward limit of the gas hydrate stability zone (LLGHSZ; ~400 m water depth). It is hypothesized that this methane may, in part, come from dissociation of gas hydrate in the underlying sediments in response to recent warming of ocean bottom waters. To evaluate the potential role of gas hydrate in the supply of methane to the shallow subsurface sediments, and the role of anaerobic oxidation in regulating methane fluxes across the sediment–seawater interface, we have characterised the chemical and isotopic compositions of the gases and sediment pore waters. The molecular and isotopic signatures of gas in the bubble plumes ($C_1/C_{2+} = 1 \times 10^4$; $\delta^{13}C\text{-}CH_4 = -55$ to $-51‰$; $\delta D\text{-}CH_4 = -187$ to $-184‰$) are similar to gas hydrate recovered from within sediments ~30 km away from the LLGHSZ. Modelling of pore water sulphate profiles indicates that subsurface methane fluxes are largely at steady state in the vicinity of the LLGHSZ, providing no evidence for any recent change in methane supply due to gas hydrate dissociation. However, at greater water depths, within the GHSZ, there is some evidence that the supply of methane to the shallow sediments has recently increased, which is consistent with downslope retreat of the GHSZ due to bottom water warming although other explanations are possible. We estimate that the upward diffusive methane flux into shallow subsurface sediments close to the LLGHSZ is 30,550 mmol m^{-2} yr^{-1}, but it is <20 mmol m^{-2} yr^{-1} in sediments further away from the seafloor bubble plumes. While anaerobic oxidation within the sediments prevents significant transport of dissolved methane into ocean bottom waters this amounts to less than 10% of the total methane flux (dissolved + gas) into the shallow subsurface sediments, most of which escapes AOM as it is transported in the gas phase.

Keywords: Methane; Seafloor sediments; Gas hydrate; Offshore Svalbard; Seabed fluxes; Anaerobic oxidation

* Corresponding author. British Antarctic Survey, Cambridge CB3 0ET, UK.
E-mail address: carolyn.graves@bas.ac.uk (C.A. Graves).

http://dx.doi.org/10.1016/j.gca.2016.11.015
0016-7037/

1. INTRODUCTION

Methane (CH_4) is a potent greenhouse gas, and its atmospheric concentration has increased by more than 10% over the past three decades (Nisbet et al., 2014). Atmospheric methane concentrations are closely correlated with temperature over glacial-interglacial cycles (e.g., Möller et al., 2013), and methane emissions may have played a key role in major climate excursions in the past, including the Paleocene-Eocene thermal maximum (e.g., Dickens, 2011; Bowen et al., 2014). Many natural sources of methane are sensitive to climatic changes including wetlands, permafrost, and methane hydrate in terrestrial and marine environments (Ciais et al., 2013). Characterization of emissions from these sources is paramount to the assessment of how levels of atmospheric methane will evolve in the context of future global climate.

Methane in marine sediments is produced by microbial and thermal degradation of organic carbon. If sediment pore waters become methane saturated, and temperature is low and pressure relatively high, then methane hydrate, an ice-like solid in which gas molecules are trapped in cages of water molecules, may form (e.g., Kvenvolden, 1993; Hester and Brewer, 2009). Methane hydrate is stable on the continental margin at water depths >200 m at high latitudes (or shallower in some permafrost settings; Krey et al., 2009) and on a global scale may contain >500 Gt carbon, although this reservoir remains poorly quantified (e.g., Milkov, 2004; Archer, 2007; Wallmann et al., 2012; Piñero et al., 2013).

A key uncertainty for climate models is the proportion of methane produced in deep marine sediments that escapes to reach the sediment–seawater interface and potentially the atmosphere. Methane rises from depth through permeable sediment strata, faults, fractures and cracks in solution, and as gas if sediment pore waters are supersaturated (Judd and Hovland, 2007). In near-surface sediments where sulphate is present, dissolved methane can be oxidised by a consortium of archaea and sulphate-reducing bacteria. This process is known as anaerobic oxidation of methane (AOM; Eq. (1); Boetius et al., 2000):

$$CH_4 + SO_4^{2-} \rightarrow HCO_3^- + HS^- + H_2O \quad (1)$$

The sub-seafloor depth interval in which methane and sulphate are consumed by AOM and concentrations of both species are nearly depleted is known as the sulphate-methane transition zone (SMTZ). The depth of the SMTZ is a qualitative proxy for the upwards methane flux into shallow sediments, as the availability of sulphate is limited by its rate of diffusion from seawater such that rapid sulphate consumption pushes the SMTZ closer to the seafloor in regions of high methane supply (e.g., Borowski et al., 1996). Hydrogen carbonate (HCO_3^-) ions produced by AOM react with calcium ions present in sediment pore waters to form calcium carbonate (Sun and Turchyn, 2014) (Eq. (2)):

$$Ca^{2+} + 2HCO_3^- \rightarrow CaCO_3 + CO_2 + H_2O \quad (2)$$

However, if the methane flux is sufficient to overwhelm the oxidising capacity of the microbial consortia (Archer et al., 2009), or the re-supply of sulphate from seawater by diffusion (Knittel and Boetius, 2009), methane is released into the water column and potentially into the atmosphere. Methane in the gas phase is not available to microbes and therefore escapes oxidation.

As the Earth and its oceans warm, there is concern that gas hydrate in marine sediments will be destabilized, releasing methane that will reinforce the greenhouse effect (e.g., Krey et al., 2009). This is supported by observations of methane bubble plumes in the water column near the landward limit of the gas hydrate stability zone (LLGHSZ), rising from sediments in which gas hydrate may have recently destabilized (e.g., Westbrook et al., 2009 (Arctic); Hautala et al., 2014 (North Pacific); Skarke et al., 2014 (North Atlantic)). Arctic regions, where climate warming is amplified (e.g. Parmentier et al., 2013), and cold bottom waters allow hydrate to form in shallow sediments where it is more susceptible to warming (e.g. Kretschmer et al., 2015), are of particular interest.

More than 200 methane bubble plumes were discovered rising from the seabed at water depths close to the LLGHZ offshore western Svalbard (Westbrook et al., 2009). In this study, we characterise the chemical composition of gases in sediments from the vicinity of the LLGHSZ offshore Svalbard, and assess the spatial distribution and temporal variability of methane fluxes into the shallow subsurface, and across the sediment–seawater interface. We examine the geochemical evidence that hydrate dissociation fuels high methane fluxes into shallow sediments, and the role of AOM in regulating methane release from the seafloor.

2. STUDY AREA AND SAMPLING

The continental margin offshore western Svalbard (Fig. 1) was shaped by the Pleistocene-Pliocene advance and retreat of the Svalbard-Barents Sea ice sheet (Sarkar et al., 2012). Glacial ice withdrew from the continental shelf about 13 thousand years ago (Elverhøi et al., 1995; Jessen et al., 2010). On the shelf and upper slope, patchy glacial sediments overlie a sequence of seaward-dipping marine sediments (Rajan et al., 2012; Sarkar et al., 2012). At water depths of more than 700 m, sediments are underlain by extensive gas hydrate deposits (Eiken and Hinz, 1993; Vogt et al., 1999; Carcione et al., 2005; Vanneste et al., 2005; Fisher et al., 2011; Sarkar et al., 2011; Bünz et al., 2012; Smith et al., 2014; Plaza-Faverola et al., 2015) that likely extend upslope to the limit of hydrate stability, although at lower hydrate concentrations (e.g., Chabert et al., 2011).

The present-day landward limit (LL) of the GHSZ (LLGHSZ) at the seabed, i.e. the shallowest water depth beneath which hydrate is stable, is defined by water depth (pressure) and the temperature of overlying bottom water of the West Spitsbergen Current (WSC) which flows northward along the upper slope. Seasonal variations in bottom water temperature are ~1.5 °C, which results in seasonal shifts in the LLGHSZ between ~360 m water depth and ~410 m water depth (Berndt et al., 2014). Critically, the WSC appears to have warmed over the last ~60 years (Westbrook et al., 2009; Ferré et al., 2012), and the present

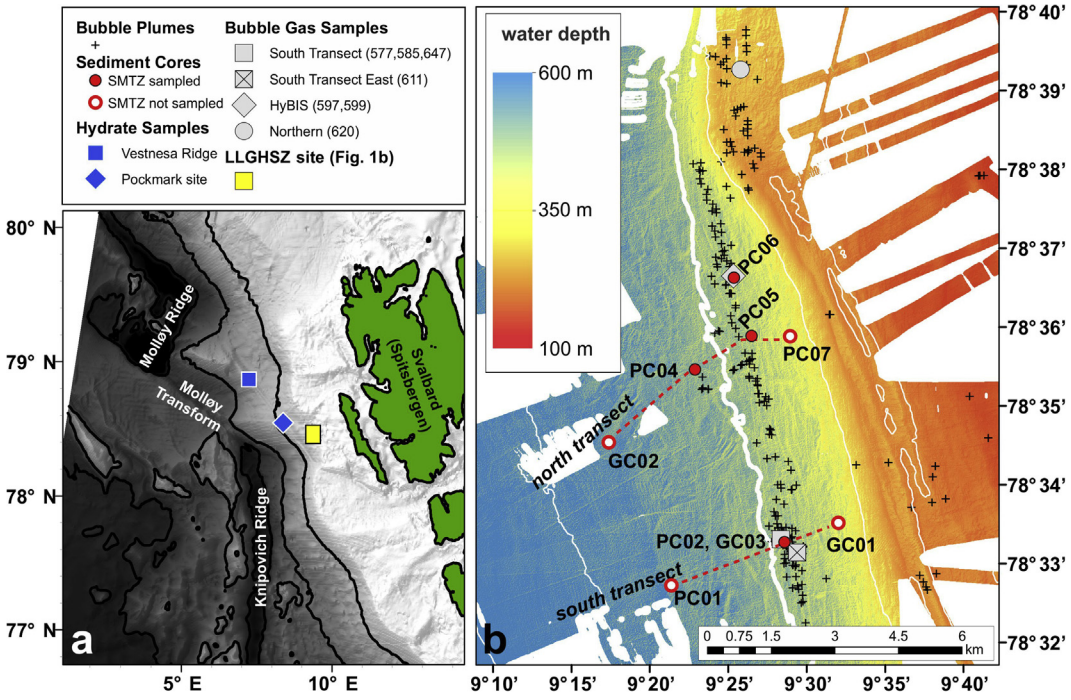

Fig. 1. Location of the West Svalbard continental margin and the study area. (a) Regional map indicating the locations of hydrate samples (blue symbols) and the main study site (LLGHSZ, yellow rectangle), bathymetry data from GEBCO (The GEBCO_08 Grid, version 20100927, http://www.gebco.net) with 1,000 m depth contours. (b) Main study site at the LLGHSZ, showing shipboard bathymetry (cruise JR253), 100 m depth contours (white lines) with 400 m in bold, seafloor gas bubble plumes mapped during JR253 (black crosses), sediment core locations (red circles), and bubble plume sampling sites (grey symbols). (For interpretation of the references to colour in this figure legend, the reader is referred to the web version of this article.)

rate of warming appears to be unprecedented in the last 2,000 years (Spielhagen et al., 2011). Warming of bottom waters results in migration of the LLGHSZ downslope to deeper waters, and release of methane from gas hydrate. Some of this methane may subsequently escape from the sediments into the overlying water column and atmosphere (e.g. Reagan and Moridis, 2007, 2009; Thatcher et al., 2013; Marín-Moreno et al., 2013, 2015).

The distribution of seafloor bubble plumes offshore western Svalbard observed during research cruise JR253 (see below) is shown in Fig. 1b. The plumes are aligned approximately along the ~400 m bathymetric contour, which coincides with the present-day LLGHSZ (Westbrook et al., 2009; Berndt et al., 2014; Sahling et al., 2014). Earlier evidence for methane emissions in this area includes observations of pockmarks (Forwick et al., 2009), and of high methane concentrations both in shallow sediments (Knies et al., 2004) and in parts of the water column (Knies et al., 2004; Damm et al., 2005). Dating of authigenic carbonates that form as a result of methane oxidation (Eq. (2)) indicates that these seafloor methane seeps have been active for more than 500 years (Berndt et al., 2014).

Sediment samples for this study were collected from the continental slope offshore Svalbard at water depths of between 320 and 460 m during RRS *James Clark Ross* cruise 253 in July and August 2011 (Table 1). Locations of methane seeps were determined using the ship's hull-mounted sonar systems (Simrad EK60 and Simrad EM122, Fig. 1b). A series of gravity and piston cores were collected, aligned roughly along two transects from water depths shallower than the LLGHSZ through the region of the seafloor bubble plumes to greater water depths within the GHSZ. Samples of gas bubbles emanating from the seafloor at the LLGHSZ were collected in a pressurized gas sampler using the manned submersible JAGO during RV *Maria S. Merian* cruise 21/4 in August and September 2012. Locations of the sediment cores and bubble plume samples are shown in Fig. 1b. Hydrate samples were collected during RRS *James Clark Ross* cruise 211 in August and September 2008 from two sites; a pockmark at 890 m water depth located ~30 km northwest of our study site ("the pockmark site"), and the Vestnesa Ridge at 1,210 m water depth (Fisher et al., 2011). Locations are shown in Fig. 1a and listed in Table 1.

3. ANALYTICAL PROCEDURES AND MODELLING

3.1. Geochemical analyses

Once retrieved to the ship, sediment cores were immediately sectioned, split, and subsampled under a nitrogen atmosphere. For gas analysis, ~3 mL of sediment was withdrawn using a cut-off plastic syringe and placed in a 20 mL glass vial containing 5 mL of 1 M sodium hydroxide to prevent microbial activity (Hoehler et al., 2000). The vials were crimp sealed and shaken vigorously to release adsorbed gases from sediment. A subsample of sediment (~3 g) was

Table 1
Locations of sampling sites. GC: gravity core, PC: piston core. MSM21/4: RV *Maria S. Merian* cruise 21/4, JR211: RRS *James Clark Ross* cruise 211, JR253: RRS *James Clark Ross* cruise 253. Distance from bubble plume estimated from shipboard mapping of bubbles by echosounder during JR253.

Cruise	Station ID	Latitude N (°)	Longitude E (°)	Sample location	Water depth (m)	Date sampled	Core length (cm)	Distance from bubble plume (km)
Sediment cores								
JR253	PC01	78:32.76	9:21.40	South transect – shallow	458	03/08/2011	379	2.6
JR253	PC02	78:33.29	9:28.57	South transect – on seep	384	04/08/2011	92	0.03
JR253	GC01	78:33.54	9:32.09	South transect – shallow	340	06/08/2011	209	1.0
JR253	GC02	78:34.58	9:17.45	North transect – deep	454	07/08/2011	360	2.5
JR253	PC04	78:35.50	9:23.00	North transect – deep seep	407	09/08/2011	343	0.02
JR253	PC05	78:35.92	9:26.63	North transect – near seep	374	10/08/2011	351	0.3
JR253	PC06	78:36.66	9:25.53	North transect – on seep	374	11/08/2011	224	0.02
JR253	PC07	78:35.91	9:29.10	North transect – shallow	323	13/08/2011	137	1.0
JR253	GC03	78:33.30	9:28.64	South transect – on seep	386	15/08/2011	162	0.01
Bubble plumes								
MSM21/4	577	78:33.34	9:28.404	South transect	394	23/08/2012	–	–
MSM21/4	585	78:33.34	9:28.411	South transect	394	24/08/2012	–	–
MSM21/4	597	78:36.68	9:25.497	HyBIS	384	25/08/2012	–	–
MSM21/4	599	78:36.68	9:25.507	HyBIS	385	25/08/2025	–	–
MSM21/4	611	78:33.17	9:29.438	South transect – eastern edge of flares	395	28/08/2012	–	–
MSM21/4	620	78:39.30	9:26.056	Northern seep region	246	29/08/2012	–	–
MSM21/4	647	78:33.34	9:28.406	South transect	394	02/09/2012	–	–
Hydrate								
JR211	33GC	78:41.07	8:16.36	Pockmark, >126 cm sediment depth	890	18/09/2008	–	–
JR211	26GC	79:00.39	6:54.26	Vestnesa Ridge, >193 cm sediment depth	1210	16/09/2008	–	–

placed in a pre-weighed plastic pot and stored at 4 °C for porosity analysis onshore. Pore waters were extracted from the remaining sediment at ~3 cm depth intervals by centrifugation under a nitrogen atmosphere, and filtered through 0.2 μm cellulose acetate filters. Subsamples for analysis of cations were stored in acid-cleaned LDPE bottles and acidified to pH 2 with thermally distilled nitric acid. Subsamples for analysis of anions were diluted by a factor of 200 with Milli-Q water, and subsamples for sulphide determination were preserved in a gelatine-zinc acetate solution. In some sampling intervals, the volume of pore water was insufficient for all analyses. Where present, gas hydrate was quickly removed from the spilt sediment core, wrapped in cotton, and stored in liquid nitrogen.

Concentrations of methane, ethane, propane, butane, isobutane, pentane, isopentane, and hexane (C_1-C_6) in sediment headspace gases were determined onboard the ship by gas chromatography with flame ionization detection (Agilent 7890, 6 Ft HayeSep Q 80/100 stainless steel column with elution of alkanes methane through hexane in 37 min achieved with a temperature program of 60 °C for 1 min., 10 °C/min. ramp to 200 °C held for 22 min.). Analytical reproducibility, based on replicate analysis of standards (20 and 100 ppm, Air Products, UK), is better than ±2%, and the detection limits are 2 ppm for C_6 and C_5, 1.5 ppm for C_4, 1 ppm for C_3, 0.6 ppm for C_2, and 0.5 ppm for C_1, which correspond to pore water concentrations of between ~0.2 μM for methane and ~0.7 μM for hexane. Reported concentrations are considered to represent minimum values because the sediments may have partly degassed during recovery. Hydrocarbon concentrations in gas bubble and hydrate samples were measured using the same method back onshore at the National Oceanography Centre (NOC) in Southampton.

The stable carbon isotope composition of methane was determined by trace gas isotope ratio mass spectrometry (IRMS, Isoprime Ltd.) at the Natural Environment Research Council Life Science Mass Spectrometry Facility at the Centre for Hydrology and Ecology in Lancaster, UK. The instrument was calibrated throughout analyses with working CH_4 standards cross calibrated with a CO_2 Ref. gas, calibrated to NIST REF-Heavy Palaeomarine Origin (CO_2) (RM 8562) and NIST REF-Biogenic Modern Biomass Origin (CO_2) (RM 8564). The reproducibility of $\delta^{13}C$-CH_4 was better than ±0.2‰. The hydrogen isotopic composition of methane was measured by Continuous Flow-Isotope Ratio Mass Spectrometry (CF-IRMS, Thermo, Delta XL) at the Institute for Marine and Atmospheric Research Utrecht, Utrecht University, following the method described in Brass and Röckmann (2010) and Sapart et al. (2011). Standardised reference air was measured before and after each set of 4 samples to correct for potential scale shifts and to calibrate the data to international standards VPDB and VSMOW. For δD, the analytical error is better than ±3.9‰. Isotope data are given in $\delta^{13}C$ and δD notation relative to, respectively, the Vienna

Pee Dee Belemnite (VPDB) and Vienna Standard Mean Seawater (VSMOW) standards.

The porosity of the sediments (ϕ) was calculated from the difference between the mass of wet sediment, and the mass of sediment after drying in an oven at ~60 °C overnight. The densities of the sediment and fluid were assumed to be 2.65 and 1.00 g cm^{-3}, respectively. For determination of total inorganic carbon and total carbon (TIC, TC), sediment subsamples were oven dried at >70 °C for >24 h, ground to a homogenous fine powder, and measured using a carbon dioxide coulometer (model CM5012, UIC Inc.) equipped with an acidification module (model CM5130), and a furnace module (model CM5120). The concentration of total organic carbon (TOC) was determined by subtracting TIC from TC. The reproducibility of these analyses is better than ±10%.

The total alkalinity of the pore waters was determined onboard ship by titration with 0.02 M hydrochloric acid, using a mixture of methyl red and methylene blue as an indicator while bubbling nitrogen through the solution. Analyses were calibrated against a seawater standard (IAPSO), and the reproducibility of the analyses is better than ±1.5%. Onshore, cation concentrations in the pore waters were determined by inductively coupled plasma optical emission spectrometry (ICP-OES, Perkin Elmer Optima 4300DV) at the NOC. The accuracy and reproducibility of this technique was assessed by multiple ($n = 3$) analyses of a seawater certified reference material (High Purity Standards™). Measured concentrations agree with certified values to within ±3%, and the reproducibility of the analyses was better than ±1% for all analytes. Anion concentrations were determined at the NOC by ion chromatography (Dionex ICS250). Reproducibility of replicate analyses is better than ±0.2% for chloride, ±2.5% for bromide, and ±1% for sulphate. Hydrogen sulphide was determined spectrophotometrically by absorbance at 670 nm following addition of *N*,*N*-dimethyl-1,4-phenylenediamine dihydrochloride and an iron(III) chloride catalyst. The working hydrogen sulphide standard was calibrated daily by titration with sodium thiosulphate against a potassium iodate standard (1.667 mM, OSIL environmental instruments and systems, UK). Reproducibility of the sulphide analyses was better than ±10%, and the limit of detection is 10 μM.

3.2. Modelling

Steady-state models of upward methane fluxes and AOM rates were applied in order to quantify the efficiency of the AOM filter, and to evaluate the validity of a steady state assumption in this setting where gas hydrate destabilization may be fuelling recent increases in methane fluxes. If sulphate is principally removed by AOM, then its pore water concentration will decrease from seawater values at the sediment–seawater interface to zero at the depth of the SMTZ (e.g., Borowski et al., 1996). At steady state, the upward diffusive flux of methane (J_{CH4}) is balanced by the downward diffusive flux of sulphate (J_{SO4}), which can be calculated using Fick's First Law (Eq. (3)):

$$J = D_0(1 - \ln(\phi^2))^{-1}\phi\left(\frac{\delta C}{\delta x}\right) \quad (3)$$

where D_0 is the diffusion coefficient of sulphate in water (1.7×10^{-10} m^2 s^{-1} at 3 °C and a salinity of 35), the term $1 - \ln(\phi^2)$ is the tortuosity correction, ø is the porosity, and $\delta C/\delta x$ is the sulphate concentration gradient (Boudreau, 1997; Mazumdar et al., 2012). Upward methane fluxes were estimated by linear least squares fitting of sulphate profiles from beneath the depth of the irrigated surface layer to the SMTZ. Profiles were linearly extrapolated to the depth of the SMTZ where this was deeper than the length of the sediment core.

Even in regions of high methane flux, oxidation of organic matter (OM) using sulphate as the terminal electron acceptor contributes to sulphate removal above the SMTZ. As a result, the simple model described above can only provide an upper limit on diffusive methane fluxes (Hoehler et al., 2000). In many cold seep environments, methane is transported by advection in upwelling fluids in addition to diffusion (e.g., Haese et al., 2003; Vanneste et al., 2011). If concentrations of methane in pore waters exceed saturation, methane will be transported in the gas phase until it reaches undersaturated pore waters. The steady-state distributions of methane and sulphate are therefore better described by partial differential equations that account for transport by diffusion, advection, and irrigation, and for reactions including sulphate reduction, methanogenesis, and AOM (Eq. (4)):

$$\left(\frac{\delta\phi C_i}{\delta t}\right) = D_i \cdot \frac{\delta}{\delta x} \cdot \left(\frac{\phi}{1 - \ln(\phi^2)} \cdot \frac{\delta C_i}{\delta x}\right) - \left(\frac{\delta\phi u C_i}{\delta x}\right) - \phi\alpha_{(x)}\left(C_{i(x)} - C_{i(0)}\right) + \phi\sum R_i \quad (4)$$

where

$$\alpha_{(x)} = \alpha' e^{-(x_b - x_{mix})},$$

$$\sum R_{SO_4} = -k_G \cdot \frac{C_{org}}{2} \cdot \frac{C_{SO_4^{2-}}}{K_{SO_4} + C_{SO_4^{2-}}} - R_{AOM},$$

$$\sum R_{CH_4} = k_G \cdot \frac{C_{org}}{2} \cdot \frac{Ki_{SO4}}{Ki_{SO_4} + C_{SO_4^{2-}}} - R_{AOM},$$

and

$$R_{AOM} = K_{AOM} C_{CH_4} \cdot \frac{C_{SO_4^{2-}}}{K_{S,AOM} + C_{SO_4^{2-}}}$$

C_i is the concentration of dissolved species i ($i = CH_4$, SO_4^{2-}), u is the advective flow velocity, $\alpha_{(x)}$ is the depth (x) dependent irrigation exchange coefficient, α' is the pore water mixing coefficient, x_b is a depth exceeding the irrigation zone, x_{mix} is the depth of the mixed layer, $(C_{i(x)} - C_{i(0)})$ is the difference between concentrations of species i at depth x and in overlying seawater ($x = 0$), ΣR_i are the reaction terms relevant for species i (Treude et al., 2003; Vanneste et al., 2011). Reactions considered are: (i) remineralisation of particulate organic matter coupled to sulphate reduction, described by the kinetic constant (k_G), organic matter concentration (C_{org}), and the half saturation constant (K_{SO4}); (ii) methanogenesis, described by k_G and

C_{org} and the inhibition constant for initiation (Ki_{SO4}); and (iii) AOM, described by the rate constant K_{AOM} and the Monod inhibition constant $K_{S,AOM}$. Information on all of these parameters is given in Table 2. The rate law formulation for AOM follows Vanneste et al. (2011), and it accounts for inhibition of methane oxidation at low sulphate concentrations. Transport of methane in the gas phase is not included in this model. Bubble formation only occurs in saturated pore waters (~76 mM CH_4 in shallow sediments at ~400 m water depth (Dale et al., 2008a; Meister et al., 2013), assuming a geothermal gradient of 0.87 °C/m (Reagan and Moridis, 2009)).

The one-dimensional transport model was solved numerically using the ordinary differential equation solver ODE15s in MATLAB®, using code described in Vanneste (2010) and Vanneste et al. (2011). The irrigation parameters α' and x_{mix} were determined by fitting the model to the upper part of the pore water sulphate profiles. The methane concentration at the lower limit of the model domain (the length of the core) was determined by fitting the depth of the modelled SMTZ to the pore water sulphate and methane profiles. The rate of AOM was determined by fitting the shape and slope of the modelled sulphate and methane profiles near the SMTZ to the measured concentrations. The fit of the model was assessed by calculating the residuals between the measured and modelled sulphate data. This model was applied only to cores where the SMTZ was sampled to allow fitting of modelled profiles to measured data in this critical interval. Steady state was reached within 10^3 years from arbitrary initial conditions using a depth step of 0.5 cm. The uncertainty of model results was assessed by sensitivity analysis of input parameters (Section 4.3).

Table 2
Transport-reaction model parameters.

Parameter	Symbol	Units	Value	Source
Diffusion coefficient for sulphate in pore water	D_{SO4}	$cm^2\ yr^{-1}$	167	Calculated for temperature, pressure, and salinity (T,P,S) conditions after Boudreau (1997), following Vanneste et al. (2011)
Diffusion coefficient for methane in pore water	D_{CH4}	$cm^2\ yr^{-1}$	273	Calculated for T,P,S conditions after Hayduk and Laudie (1974), following Vanneste et al. (2011)
Concentration of species i ($i = CH_4$, SO_4^{2-}) at depth x	$C_{i(x)}$	mM	-	Depth profiles, fit to measured data (see Fig. 5)
Bottom seawater methane concentration	$C_{CH4(0)}$	mM	0.00	Measured concentration in near-surface sediments
Bottom seawater sulphate concentration	$C_{SO4(0)}$	mM	28	Measured concentration in near-surface sediments
Core-bottom sulphate concentration	C_{SO4}^{bottom}	mM	0	Measured core-bottom concentration
Core-bottom methane concentration	C_{CH4}^{bottom}	mM	-	Used as fitting parameter for methane concentration profiles (see Table 4)
Porosity	ϕ	–	0.5	Average measured value (see Supplemental Fig. 1 and discussion in Section 4.3)
Pore water advection	u	$cm\ yr^{-1}$	0.03	Sedimentation rate from Jessen et al. (2010); see discussion in Section 4.3 and Supplemental Figs. 4 and 5, and Supplemental Tables 2 and 3.
Pore water mixing coefficient	α'	yr^{-1}	10	Fit to measured sulphate concentration depth profiles, and kept constant between cores
Depth of irrigation mixing	x_{mix}	cm	5–30	Fit to measured sulphate concentration depth profiles (see Table 4)
Depths exceeding mixing zone	x_b	cm	–	Model domain beneath irrigation mixing zone
Rate constant for organic matter remineralisation	k_G	yr^{-1}	1×10^{-6}	As in Vanneste et al. (2011)see discussion in Section 4.3
Organic carbon content	C_{org}	mM	1300	Average measured value (0.6 ± 0.3 wt.%) expressed as mmol per L of dry sediment for sediment density of $2.65\ g\ mL^{-1}$. (see Supplemental Fig. 2 and discussion in Section 4.3)
Half saturation constant for sulphate reduction coupled to organic matter remineralisation	K_{SO4}	mM	1	as in Vanneste et al. (2011), value is assumed due to absence of constrains available for natural systems
Inhibition constant for initiation of methanogenesis	Ki_{SO4}	mM	1	As in Vanneste et al. (2011), value is assumed due to absence of constrains available for natural systems
Rate constant for anaerobic oxidation of methane	K_{AOM}	yr^{-1}	-	Fit to measured sulphate and methane concentration depth profiles within the SMTZ (see Table 4 and Supplemental Table 3)
Monod inhibition constant for AOM	$K_{S,AOM}$	mM	1	As in Vanneste et al. (2011), based on data from Nauhaus et al. (2002)

4. RESULTS

4.1. Chemical and isotopic composition of gas bubble plumes and hydrate

The molecular composition (C_1/C_{2+}) and methane stable carbon ($\delta^{13}C$-CH_4) and hydrogen (δD-CH_4) isotope compositions of the gas bubble plumes at the LLGHSZ, and samples of gas hydrate from sites closest to the bubble plumes (Vestnesa Ridge and the 'pockmark' site) are given in Table 3, along with previously reported data (C_1/C_{2+} and $\delta^{13}C$-CH_4 only). Note that no hydrate was recovered in any of our sediment cores from the LLGHSZ sites, including those located within the GHSZ (cores PC01, GC02 and PC04). The absence of hydrate in the cores outside the GHSZ is not surprising. The observed methane concentrations in the three within-GHSZ cores additionally rule out hydrate occurrence in those sediments: hydrate is only stable very close to the sediment–seawater interface at these water depths (estimated for geothermal gradients of 0.87 to 0.7 °C/m (Reagan and Moridis, 2009; Westbrook et al., 2009) and bottom water temperature of 3 °C using the gas hydrate stability curve of Dickens and Quinby-Hunt (1994)). This interval of hydrate stability is above the SMTZ so methane concentrations are low and hydrate formation is prohibited.

4.2. Chemical composition of sediment pore waters

The SMTZ was sampled in 5 of the 9 sediment cores recovered near the LLGHSZ (pore water data shown in Fig. 2, core locations in Fig. 1). The depth of the SMTZ is relatively shallow (<300 cm below the seafloor) in the vicinity (within 30 m) of the methane seeps. Cores recovered from 1 to 3 km away from the LLGHSZ, at both shallower and deeper water depths, did not sample the SMTZ.

Sulphate profiles are nearly linear above the SMTZ, decreasing from seawater values (28 mM) to <1 mM (Fig. 2). Below the SMTZ, methane concentrations are above 1.8 mM (methane saturation under surface conditions of ~4 °C and 1 bar), and sediment degassing following core recovery is expected. Methane concentrations are

Table 3
Molecular and isotopic composition of bubble plume and hydrate gas. Sample locations are listed in Table 1 and shown in Fig. 1. Bubble plume samples for this study are from cruise MSM21/4: RV *Maria S. Merian* cruise 21/4 (2012), and hydrate samples from cruise JR211: RRS *James Clark Ross* cruise 211 (2008). Hydrate $\delta^{13}C$-CH_4 data from Fisher et al. (2011). Uncertainty of $\delta^{13}C$-CH_4 and δD-CH_4 measurements of bubble plume samples is reported as the standard deviation of three subsamples; uncertainty of $\delta^{13}C$-CH_4 measurements of hydrate is reported as the standard deviation of analyses of three separate pieces of hydrate from an individual core.

Station ID	Station location	C_1/C_{2+} (mol/mol)	$\delta^{13}C$-CH_4 (‰)	δD-CH_4 (‰)
Bubble plumes				
577	South transect	9.8×10^3	-54.6 ± 0.3	-187 ± 1
585	South transect	9.6×10^3	-54 ± 1	-179 ± 3
597	HyBIS	1.1×10^4	-51.1 ± 0.8	–
599	HyBIS	1.2×10^4	-51.3 ± 0.1	-178 ± 2
611	South transect, east	1.2×10^4	-51.6 ± 0.1	–
620	Northern	1.1×10^4	-55.5 ± 0.4	187.0 ± 0.1
647	South transect	9.7×10^3	-55.0 ± 0.5	–
Sahling et al. (2014)	Northern*	1.5×10^4	−55.8	–
Sahling et al. (2014)	South transect	9.7×10^3	−56.0	–
Hydrate				
33GC	Pockmark site	500	-54.6 ± 2	-174 ± 4
26GC	Vestnesa Ridge	60	-45.7 ± 3	-180 ± 2
Smith et al. (2014)	Vestnesa Ridge	26	−47.7	–

* Sahling et al. (2014) data for the northern sampling site is the average of two samples reported for this location.

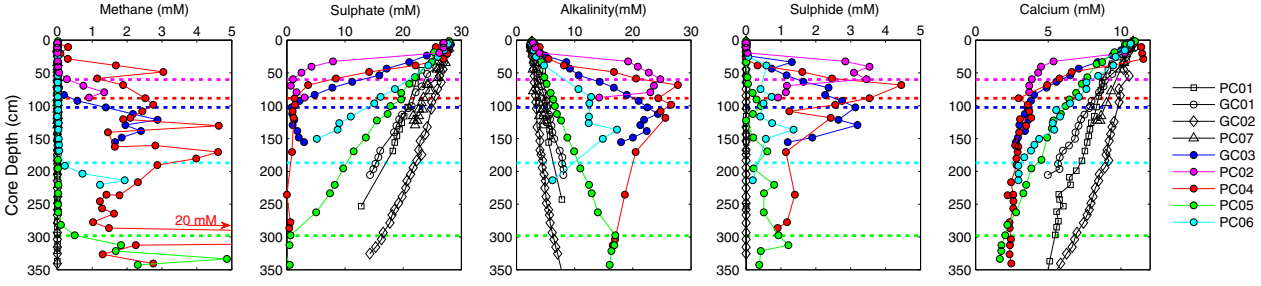

Fig. 2. Profiles of pore water methane, sulphate, alkalinity, sulphide and calcium. Cores collected from less than ~0.01 to 0.3 km away from bubble plumes are shown by the coloured symbols. Dashed horizontal lines indicate the depth of the SMTZ, where sampled. Sulphide was not determined in cores GC01 and PC07. (For interpretation of the references to colour in this figure legend, the reader is referred to the web version of this article.)

generally less than 20 μM in the presence of more than 1 mM sulphate, with the exception of core PC04 where methane concentrations are >1.8 mM up to 40 cm below the seabed, even in the presence of >20 mM sulphate (Fig. 2). The concentration of dissolved sulphate is close to bottom seawater in the uppermost 20 to 30 cm of the sediment column in cores PC02 and PC04, which is indicative of seawater drawdown into the sediments (irrigation; Fig. 2).

Depth profiles of pore water alkalinity and sulphide confirm that AOM occurs in sediments at the depth of the SMTZ (Fig. 2; Eqs. (1) and (2)). Total alkalinity increases with depth from a seawater value of ~2.3 mM to 12–25 mM at the SMTZ due to production of HCO_3^- and, to a lesser extent, HS^- (Fig. 2, Eq. (1)). Hydrogen sulphide (Fig. 2) was only detected in pore waters from cores that sampled the SMTZ (GC03, PC02, PC04, PC05 and PC06), reaching ~4 mM in cores with the shallowest SMTZ (PC02 and PC04). Sulphide was not measured in cores GC01 and PC07. Calcium concentrations decrease abruptly at the SMTZ (Fig. 2), likely due to the formation of authigenic calcium carbonate (Eq. (2)). Carbonate nodules were recovered in the five cores where the SMTZ was sampled.

At all but one site (PC04) where the SMTZ was sampled, lowest δ^{13}C-CH_4 values (−84 to −97‰) occur within the depth interval where AOM rates are highest (Fig. 3). By contrast, core PC04 is characterised by relatively high δ^{13}C-CH_4 values (up to −20‰) immediately above the depth of the SMTZ (Fig. 3). Above the SMTZ, δ^{13}C-CH_4 values are ~−45 ± 2.5‰ (average and standard deviation of 36 samples from cores PC01 and GC01). Below the SMTZ, where methane concentrations increase, δ^{13}C-CH_4 values approach those measured in bubble plume gases sampled at the seafloor (Fig. 3; Table 3).

Concentrations of species that are not produced or consumed during shallow diagenetic reactions (chloride: Cl^-, bromide: Br^-, and sodium: Na^+) show little variation with depth at all sampling sites, whether close to or distant from seafloor bubble plumes (Fig. 4). The average and standard deviation of all of Cl^- measurements is 537 ± 14 mM. In core PC04, 7 of the 16 pore water samples from close to the sediment–seawater interface, which have high methane concentrations, have slightly lower than average Cl^- concentrations (i.e. by more than two standard deviations). Three of these 16 pore water samples are also slightly enriched in Br^- (940–1010 μM, compared to the average of 850 ± 24 μM for all other pore water samples). Two of these samples also have low Cl^-, and one has a seawater sulphate concentration.

4.3. Methane flux modelling

Results of methane flux modelling for both the diffusion-only and the transport-reaction (TR) models are shown in

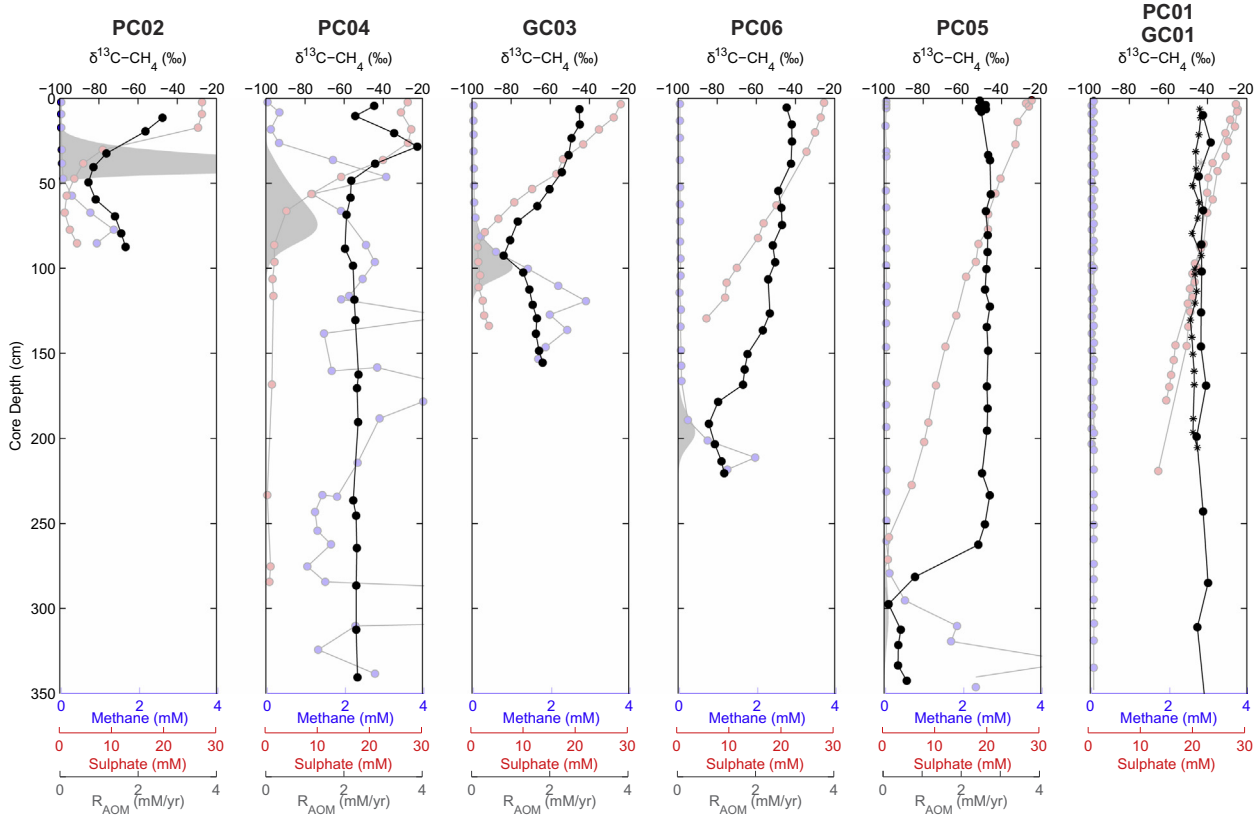

Fig. 3. Profiles of sediment methane carbon isotopic ratio (δ^{13}C-CH_4). Profiles of methane (blue) and sulphate (red) concentrations, and modelled rates of anaerobic oxidation of methane (grey shaded areas, see Section 4.3) are also shown. (For interpretation of the references to colour in this figure legend, the reader is referred to the web version of this article.)

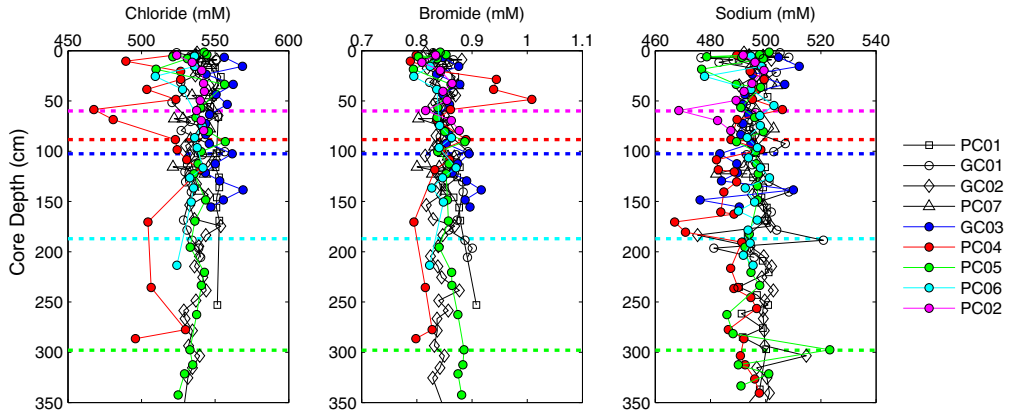

Fig. 4. Pore water profiles of chloride, bromide and sodium. Cores collected from less than ~0.01 to 0.3 km away from active bubble seeps are shown by the coloured symbols. Dashed horizontal lines indicate the depth of the SMTZ, where sampled.

Fig. 5, and values of the input and output parameters are given in Table 4.

The average porosity of the sediments is 0.47 ± 0.09, and the average TOC content is 0.6 ± 0.3wt%. Neither variable shows systematic variation with depth, or core location (Supplemental Figs. 1 and 2). For this reason, these average values were applied in the methane flux models.

The relatively low TOC content of the sediments supports the use of the diffusion-only model, which assumes that OM remineralisation is not a significant sulphate sink. Moreover, low rates of OM remineralisation are obtained with the TR model (see Table 4), and are in agreement with the results of Pohlman et al. (2013) who showed that the absence of significant sulphate removal by OM-remineralisation can enhance methane oxidation in OM-poor glaciogenic sediments. Sulphate and methane profiles and flux estimates are insensitive to halving or doubling either k_G or TOC in the TR model. Increasing k_G by an order of magnitude or more leads to concave up sulphate profiles that are not consistent with observations, as well as depletion of sulphate above the depth of the observed SMTZ, even if the methane concentration at the bottom of the core ($CH_{4bottom}$) is reduced to zero.

For the TR model, sediment porosity has a significant effect on the modelled methane flux into the SMTZ: if porosity is increased by 0.09 (the standard deviation of the measured values), then both the flux of methane into the sediment column and the rate of AOM increase by ~40%, while decreasing porosity by the same amount reduces the methane flux and rate of AOM by ~20% (Supplemental Table 1). Modelled pore water profiles and AOM efficiency are not significantly affected by porosity, but irrigation fluxes can change by as much as +70 to −50% for PC02. However, the irrigation flux is small compared to the rate of AOM and the total methane flux across the sediment–seawater interface in this area (Section 5.3).

We could not determine the pore water advection term (u) by curve fitting to conservative species such as Cl^- and Na^+ (e.g. Vanneste et al., 2011) as these show no definitive evidence for upward advective flow of pore waters with a different chemical composition (Fig. 4). If we assume that advective flow is not important, u is simply equal to the sedimentation rate (~0.03 cm/year; Jessen et al., 2010) because porosity is assumed to be constant and compaction can therefore be neglected (Malinverno and Pohlman, 2011). Doubling or halving u changes the modelled methane flux by <1%. If u is increased by more than an order of magnitude, modelled sulphate profiles have a slight concave up shape, and the methane concentration at the bottom of the core ($CH_{4bottom}$) must be significantly decreased to maintain the depth of the SMTZ.

With the exception of the two cores with the shallowest SMTZ (PC02 and PC04), the measured sulphate profiles show no curvature, which supports our interpretation that advective flow is insignificant. For PC04, a good fit is obtained by increasing the advective flux by an order of magnitude (to 0.3 cm yr^{-1}) and simultaneously decreasing $CH_{4bottom}$ by one third, the combined effect of this on all of the model output parameters of interest is negligible (Supplemental Fig. 3; Supplemental Table 2). It is important to note, however, that even the reduced modelled $CH_{4bottom}$ value for PC04 is higher than the *in situ* methane solubility (~80 mM, calculated for *in situ* S, T, P conditions following Dale et al., 2008a). This implies a contribution from methane in the gas phase that is not described by the TR model (Vanneste, 2010). We consider the effects of adding a gas phase term (following Meister et al., 2013) in Supplemental Fig. 4 and Supplemental Table 3. Again, we are able to conclude that this has only a small effect on both the methane flux across the sediment–seawater interface (increase from 70 to 110 mmol m^{-2} yr^{-1}), and the rate of AOM at the SMTZ (increase from 240 to 280 mmol m^{-2} yr^{-1}). For core PC02, a good fit to the measured sulphate data can be achieved by increasing the advective fluid flow more than 100-fold (to 5 cm yr^{-1}), and reducing $CH_{4bottom}$ to 1.5 mM (Supplemental Fig. 5; Supplemental Table 4). Although such high advective flows have been observed in mud volcano settings (e.g., Vanneste et al., 2011), all of the other sites sampled in this study are consistent with low rates of pore water advection, including core GC03 which is only ~30 m from PC02. Additionally, a value of 1.5 mM for $CH_{4bottom}$ is less than the methane saturation concentration, which is usually achieved in sediments below the SMTZ, suggesting that the bottom

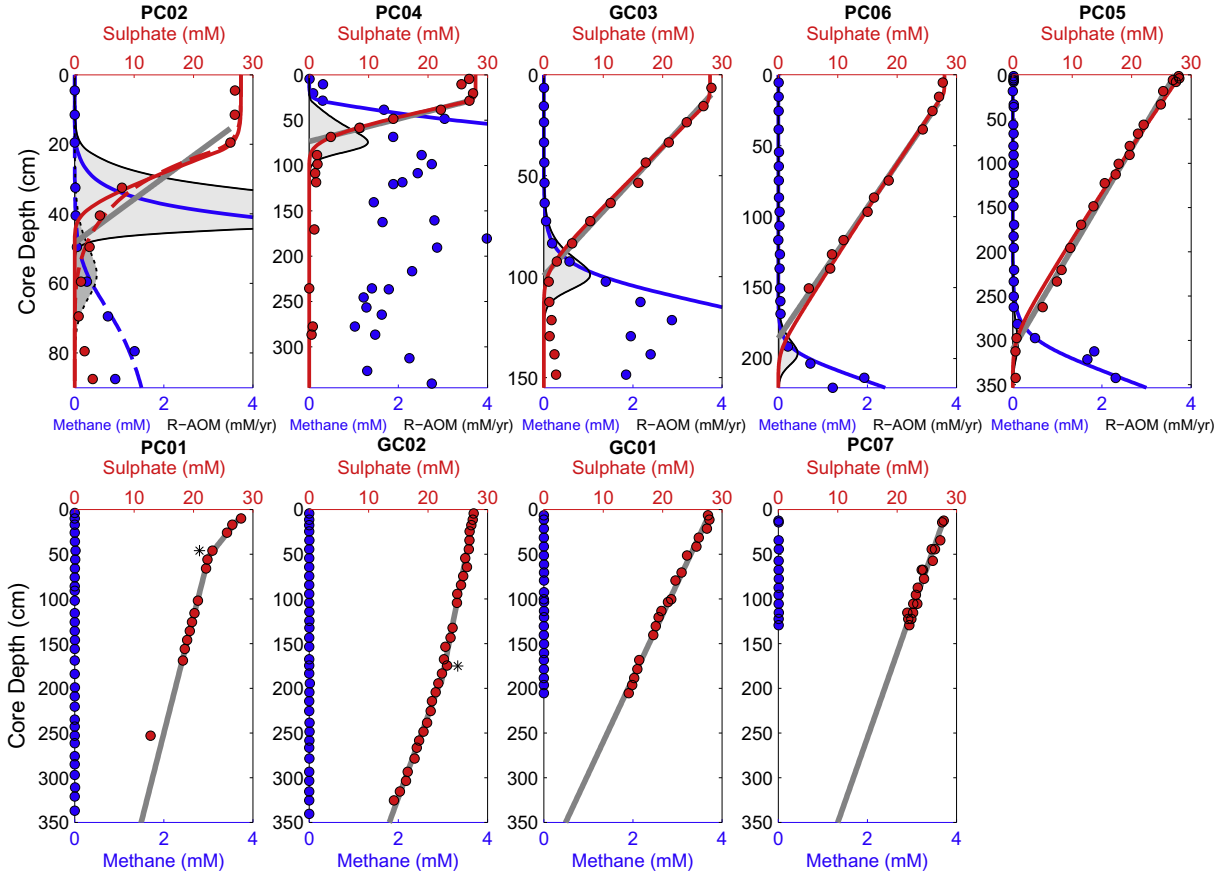

Fig. 5. Modelled pore water profiles: methane (blue), sulphate (red) and anaerobic methane oxidation rate (R_{AOM}, grey shading). Measured data are shown by the coloured circles. Results of the diffusion-only model are shown by the solid grey lines (sulphate only, R^2 values given in Table 4). Results for the transport-reaction model for sulphate and methane are shown, respectively, by the red and blue lines. Black dashed lines for PC02 show the results of transport-reaction modelling with high advective flow (see Table 4). The maximum rate of AOM rate modelled in core PC02 is 9.9 mM yr^{-1} (30 nmol cm^{-3} day^{-1}). (For interpretation of the references to colour in this figure legend, the reader is referred to the web version of this article.)

boundary is within the interval affected by AOM. The rate constant of AOM (K_{AOM}) only has a significant effect on the modelled methane concentration profile when a high advective flow is imposed (Supplemental Fig. 6; Supplemental Table 4). It is difficult to compare K_{AOM} values from different modelling studies, because the models differ and the rate constants incorporate a range of site-specific physical parameters (e.g., Regnier et al., 2011). The K_{AOM} values obtained by fitting to the methane profile at the SMTZ (0.2–5 yr^{-1}; Table 4) are slightly lower than values obtained with the same model for the Carlos Ribeiro mud volcano (7–25 yr^{-1}; Vanneste et al., 2011), which likely reflects the different seafloor seepage environments. Modelled rates of AOM at the STMZ are 0.3–30 nmol cm^{-3} day^{-1} (Fig. 5), within the range of those measured elsewhere in coastal and margin sediments (0.1–50 nmol cm^{-3} day^{-1}; Knittel and Boetius, 2009).

There is good agreement between methane flux results from the diffusion only and TR models for cores with moderate rates of methane seepage (GC03, PC05, PC06; Table 4). The absence of significant OM remineralisation and low values of u in the TR model supports the use of the diffusion-only model to estimate methane fluxes by extrapolation of the linear sulphate profiles in cores GC01 and PC07. However, the two cores recovered at deeper water depths (~450 m) within the GHSZ (PC01 and GC02) have kinked sulphate profiles that cannot be reproduced by the diffusion-only model, so methane fluxes have been estimated by applying separate linear fits to the upper and lower segments (Fig. 5). The direction of the shift in the sulphate gradient is different for the two cores, with a steeper sulphate profile (shallower inferred SMTZ) in the uppermost sediments of PC01 and a steeper profile in the deeper sediments in GC02. In PC01, the sulphate gradient observed in the uppermost sediments implies that the SMTZ should be located within the sampled core, and demonstrates how the methane flux would have been overestimated by the diffusion-only model if the recovery depth of this core was shorter and the sulphate profile assumed linear.

Agreement between the two models is poor for the two cores with the shallowest SMTZ (PC02 and PC04, Table 4). Both models provide a good fit to the sulphate profile for core PC04, but the methane fluxes into the base of the

Table 4
Values of input and output parameters for the diffusion and transport-reaction models. Depth of SMTZ and sulphate/methane fluxes estimated using the diffusion model for cores GC02 and PC01 are provided by considering the fit of the model both above, and below, the kink in the sulphate profile. Values in bold highlight the calculated methane flux to the shallow subsurface sediments for each model.

Parameter	Units	PC02	PC02*	PC04	GC03	PC06	PC05	GC01	PC07	GC02	PC01
Diffusion model											
SMTZ	m	0.5		0.7	1.0	1.9	3.1	4.0	5.5	9.5; 5.8	2.4; 6.4
Fit (R^2)	–	0.86		0.99	0.99	1.00	0.99	0.99	0.95	0.98	0.99
Downward diffusive sulphate flux (J_{SO4}) = upward methane flux to SMTZ	mmol m^{-2} yr^{-1}	**250**		**190**	**100**	**50**	**30**	**20**	**15**	**10; 20**	**40; 10**
Transport-reaction model inputs											
[CH_4] at bottom of core	mM	50	1.5	150	12	2.4	3	–	–	–	–
Irrigation depth (x_{mix})	cm	22	22	30	15	15	5	–	–	–	–
AOM rate constant (K_{AOM})	yr^{-1}	5	5	0.2	2	3	0.5	–	–	–	–
Transport-reaction model outputs								–	–	–	–
Methane flux to shallow subsurface sediments	mmol m^{-2} yr^{-1}	**550**	**50**	**310**	**120**	**50**	**30**	–	–	–	–
Methanogenesis	mmol m^{-2} yr^{-1}	0.2	0.1	0.9	0.2	0.1	0.3	–	–	–	–
AOM rate	mmol m^{-2} yr^{-1}	540	50	240	120	50	30	–	–	–	–
SO_4 reduction rate for OM remineralisation	mmol m^{-2} yr^{-1}	0.1	0.2	0.2	0.3	0.6	0.9	–	–	–	–
Methane flux to seawater by irrigation	mmol m^{-2} yr^{-1}	10	0.09	70	0	0	0	–	–	–	–
Methane flux to seawater by diffusion	mmol m^{-2} yr^{-1}	0.01	0.0004	0.02	0.0004	0.0003	0.0009	–	–	–	–
Ratio of modelled methane flux to linear diffusion model result	–	**2.2**	**0.2**	**1.7**	**1.2**	**1.0**	**1.1**	–	–	–	–

* Pore water advection (u) increased from 0.03 cm yr^{-1} to 5 cm yr^{-1}.

SMTZ disagree by a factor of 1.7 with the TR model yielding the higher value. In core PC02, the sulphate profile is slightly concave down and therefore poorly modelled by the diffusion-only model (Table 4). The TR model best reproduces both the sulphate and methane profiles when a high upward advective flux of pore water with 1.5 mM methane is applied but, as described above, these conditions are unlikely. The best TR model fit to the sulphate data without high advection (solid line in Fig. 5) disagrees with the diffusion only model methane flux, yielding more than double the methane flux to shallow subsurface sediments (Table 4).

In the TR model, the relatively shallow SMTZ combined with the relatively deep seawater irrigation depth in PC04 leads to a small flux of methane to the overlying seawater by irrigation (Table 4). An irrigation flux is also modelled for core PC02, if the advection rate is low (Fig. 5, Table 4).

5. DISCUSSION

5.1. Origin of methane at the landward limit of the GHSZ

Ascertaining the origin of the gas that fuels the seafloor bubble plumes at the LLGHSZ is challenging. In agreement with other studies conducted in this area (Sahling et al., 2014), the gas bubbles have high C_1/C_{2+} values and higher hydrocarbons (C_{3+}) are absent, which is consistent with a microbial gas source. However, the δ^{13}C-CH_4 signatures of bubble plume samples are slightly higher than usual for marine microbial methane (carbonate reduction, Fig. 6). The combined C_1/C_{2+} and δ^{13}C-CH_4 data do not indicate simple mixing between gas of microbial and thermogenic sources (Fig 6a). In an effort to provide further constraints on the origin of the bubble plume methane gas, we also conducted δD-CH_4 analyses, but these data are consistent with both a thermogenic and a microbial (carbonate reduction) source (Fig. 6b).

It has been proposed that the δ^{13}C-CH_4 values of seafloor bubble plumes at the LLGHSZ are higher than is usual for marine microbial methane due to mixing with methane enriched in ^{13}C such as that which has undergone oxidation within the sediments (Sahling et al., 2014). We suggest that oxidation is unlikely, for two reasons. First, the molecular and isotopic compositions of the gas bubbles are the same as methane in sediments recovered from below the SMTZ (core PC04, Fig. 3), where oxidation is not expected to be significant because sulphate (and oxygen) are absent. Second, our δ^{13}C-CH_4 and δD-CH_4 data indicate that the carbon and hydrogen isotopic compositions of methane in the bubble plumes are inconsistent with oxidation of a microbial source (that has typical δ^{13}C-CH_4 and δD-CH_4 values; Fig. 6b).

δ^{13}C-CH_4 values of headspace gas in sediments on the shelf have been interpreted as evidence for isotopic fractionation of methane during slow upward gas migration along

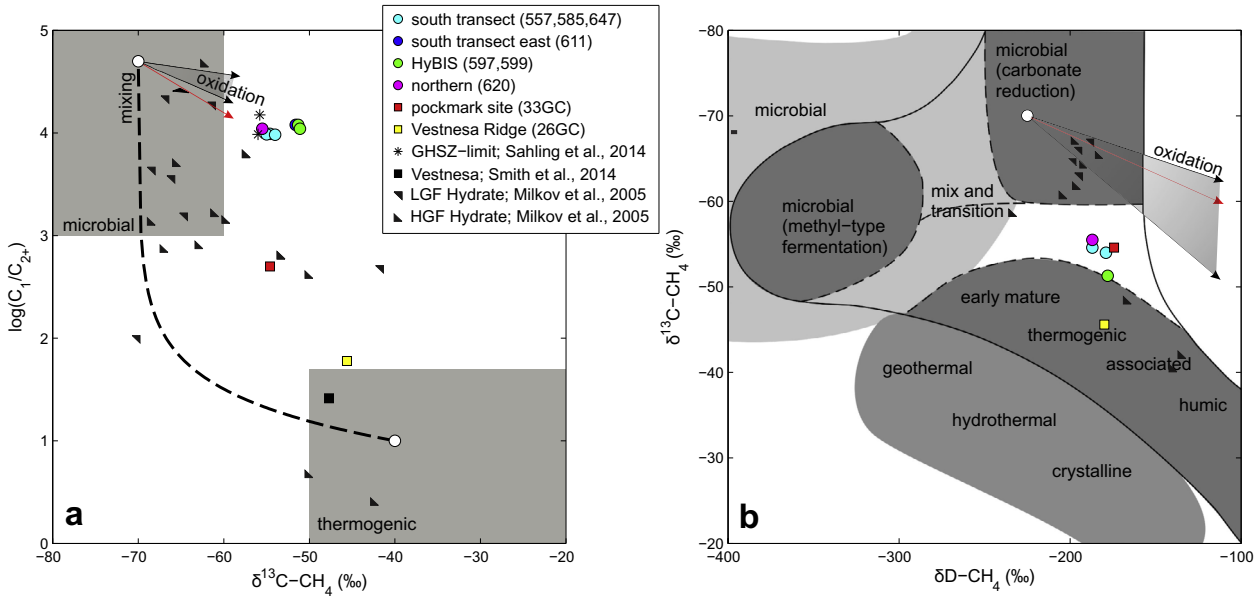

Fig. 6. Molecular and isotopic composition of hydrate and bubble plume gases from this study (coloured symbols) and others (black symbols). (a) 'Bernard diagram' modified after Whiticar (1999), (b) Cross plot of methane carbon and hydrogen isotopic data with classification according to Whiticar (1999) White open circles indicate typical end member microbial (δ^{13}C-CH$_4$: −70‰, C_1/C_{2+}: 50,000, δD-CH$_4$: −225‰, in A and B) and thermogenic (A only: δ^{13}C-CH$_4$: −40‰, C_1/C_{2+}: 10) source signatures, connected by a black dashed mixing line (A only). Shaded area between the black arrows shows the effect of oxidation on δ^{13}C-CH$_4$ and δD-CH$_4$ for the range of isotope fractionation factors (α_C for carbon and α_D for hydrogen) reported from laboratory experiments with aerobic and anaerobic methanotrophic bacteria (Feisthauer et al., 2011; α_C: 1.012–1.036, α_D: 1.093–1.320). Red arrows show α_C and α_D values measured in aerobic sediments from the northern Baltic Sea (Egger et al., 2015; α_C: 1.009, α_D: 1.098). Vestnesa Ridge hydrate δ^{13}C-CH$_4$ data are from Fisher et al. (2011). Previously reported Vestnesa Ridge hydrate (Smith et al., 2014), and LLGHSZ bubble plume data (Sahling et al., 2014), as well as hydrate data from both high gas flow (HGF) and low gas flow (LGF) regions (Milkov et al., 2005), are also shown. (For interpretation of the references to colour in this figure legend, the reader is referred to the web version of this article.)

faults in subsurface sediments (Damm et al., 2005). Faster migration of lighter species during diffusive transport through sediments could strip both the heavier hydrocarbons and heavier isotopes (^{13}CH$_4$ and D-CH$_4$) from thermogenic gas moving from deeper in the sediment column or through seaward-dipping prograding marine sequences towards the LLGHSZ (Schoell, 1983). The rate of fractionation depends on the mass difference between molecules and isotopologues, and the tortuosity of the sediment pores through which gases travel (Prinzhofer and Pernaton, 1997). Thus, the effect on C_1/C_{2+} may be much more significant in natural settings than isotopic fractionation, however it is not clear if migration alone could produce the observed geochemical signature in this setting (Fuex, 1980; Schoell, 1983; Prinzhofer and Pernaton, 1997; Zhang and Krooss, 2001; Nuzzo et al., 2009). A contribution from this mechanism is, however, supported by seismic reflection data in the study area which shows evidence for the migration of free gas up the continental slope (Westbrook et al., 2009; Hustoft et al., 2009; Rajan et al., 2012; Sarkar et al., 2012; Thatcher et al., 2013).

The overall seaward dip of the sediment strata in the continental slope favours the landward migration of free gas which accumulates at the base of the hydrate stability zone offshore western Svalbard (e.g. Sarkar et al., 2012) and, at culminations such as the Vestnesa Ridge, thermogenic gas escapes through pockmarks into the water column (Bünz et al., 2012; Smith et al., 2014). *In situ* biogenic methanogenesis is likely at the base of the hydrate stability zone, where temperatures are 5–70 °C, while the increase in geothermal gradient with increasing distance offshore (Vanneste et al., 2005) favours thermogenic gas production at comparatively shallow depths near the foot of the continental slope (Dumke et al., 2016). The proportion of glaciogenic sediments with very low permeability increases towards the top of the continental slope, but the greater part of the well-stratified marine sequence containing free gas continues beneath these glacigenic sediments (Rajan et al., 2012; Sarkar et al., 2012; Thatcher et al., 2013), providing a source of gas under the uppermost continental slope and shelf.

Consequently, although the actual sources of the gas cannot, at present, be identified, it is improbable that the gas is primarily from local in-situ production, although we acknowledge that a number of other potential methane sources are possible. These include: microbial methane produced from a ^{13}C-enriched CO_2 source (e.g., Claypool et al., 1985), abiotic methane produced during the serpentinization of ultramafic rocks further offshore western Svalbard (Johnson et al., 2015), and methane associated with onshore coal deposits and other hydrocarbon sources (e.g. Roy et al., 2015). To resolve this issue more comprehensive analysis of gases in shallow sediments in this area is required, such as δ^{13}C-C_2H_6 (e.g. Milkov, 2005),

$\delta^{13}C\text{-}CO_2$ (Pohlman et al., 2009), and methane clumped isotopes (Wang et al., 2015).

5.2. Evaluation of evidence for gas hydrate dissociation offshore western Svalbard

5.2.1. Evidence from the composition of bubble plumes and pore waters at the LLGHSZ

Recent warming of overlying bottom waters at the LLGHSZ means that gas hydrate – if present – is unstable and either currently dissociating or has recently dissociated (e.g. Berndt et al., 2014). Gas released from methane hydrate should have lower C_1/C_{2+} than the gas from which the hydrate formed, because heavier hydrocarbons are slightly enriched in the hydrate phase during gas hydrate formation (e.g. Sloan, 1998). This molecular fractionation can be used as a tool to determine if seafloor bubble plume gas is sourced from hydrate dissociation (e.g. Pape et al., 2010). However, without a sample of methane hydrate from the immediate vicinity of the LLGHSZ, a direct comparison with the bubble plume molecular composition is not possible. The bubble plume gasses have a slighter higher C_1/C_{2+} than hydrate recovered within the GHSZ ~30 km northwest of the LLGHSZ at the 'pockmark' site: $9.6–12 \times 10^3$ compared to 5×10^2 (Fig. 6a, Table 3). The C_1/C_{2+} ratio for the gas from which this hydrate formed is calculated to be 3.6×10^3 (Sloan, 1998; Smith et al., 2014), slightly lower than the ratio measured in the bubble plume gases. If the bubble plume gases are derived from hydrate, the gases which formed that hydrate would have $C_1/C_{2+} > 5 \times 10^4$. Considering the range of C_1/C_{2+} in the bubble plume gases and for hydrate samples from offshore Svalbard (Table 3), we must therefore conclude that C_1/C_{2+} analyses provide no evidence to support (or refute) escape of methane from a hydrate source across the sediment–seawater interface at this site.

Hydrate formation and dissociation also alters the salinity of surrounding pore waters. Chloride concentrations are reduced by dilution with relatively fresh water released from hydrate, as observed in sediment cores where hydrate was destabilized during recovery (e.g., Egeberg and Dickens, 1999; Tréhu et al., 2004; Panieri et al., 2014). Pore water can also become chloride enriched during hydrate formation (e.g., Haeckel et al., 2004). Of the nine sediment cores recovered, only one (PC04) has pore water chloride concentrations that differ from seawater: low chloride concentrations were observed both above and below the sulphate reduction zone (Fig. 4). Site PC04 is located just inside the summertime GHSZ, which extended to ~80 cm sediment depth at the time of sampling; pore waters in this interval have high sulphate concentrations which precludes the formation of gas hydrate. However, high methane concentrations are found above this depth (up to ~40 cm), which may indicate a non-steady state situation (see Section 5.2.2). Interpretation of pore water data from core PC04 is further complicated by the presence of pore waters enriched in bromide (Fig. 4), which is not consistent with pore water dilution, but with input from organic matter degradation that presumably occurs at depth within these sediments (e.g., Egeberg and Dickens, 1999; Fehn et al., 2006). However, the overall shape of the bromide profile is not indicative of pore water advection from depth. Therefore, as with the bubble plume gas C_1/C_{2+}, analyses of porewater chloride and bromide concentrations to not unequivocally support (or refute) a hydrate source for methane in the near-surface of core PC04.

5.2.2. Temporal variability of methane supply to the shallow subsurface sediments

If seafloor methane bubble plumes at the LLGHSZ are fuelled by hydrate dissociation, then the methane flux into shallow subsurface sediments should vary in response to the movement of the landward limit of the GHSZ due to changes in ocean bottom water temperatures on both seasonal and multi-decadal timescales (e.g., Marín-Moreno et al., 2015). In all but one of the sediment cores recovered from the vicinity of the LLGHSZ (PC05, PC06 and GC03) we observed linear pore water sulphate profiles ($R^2 > 0.95$; Table 5; Fig. 5). These profiles are consistent with steady-state sulphate diffusion down to the SMTZ. If temperature-driven dissociation of localized pockets of shallow methane hydrate is fueling the seafloor bubble plumes, then none of the cores from the LLGHSZ record the variability in methane fluxes expected to be associated with this process. Furthermore, the two sites at shallower water depths where bubble plumes are not observed (GC01 and PC07) also show no evidence for a reduction in supply of methane to the shallow sediments, which would be expected if the GHSZ had shifted downslope as a result of recent warming (e.g., Ferré et al., 2012). This suggests that the supply of methane to the sediments has been stable, despite local changes in hydrate stability. Changes in methane flux generate non-linear sulphate profiles that persist for up to several thousand years (Hensen et al., 2003; Henkel et al., 2011).

Core PC02 is a possible exception. Its pore water sulphate profile is poorly approximated by steady-state diffusion ($R^2 = 0.86$), and achieving a good fit with the transport reaction model requires imposing a high value for u (Fig. 5; Table 5). Because the TR model results are likely influenced by the short model domain (Section 4.3), the poor fit of the steady-state model could be interpreted to reflect a decrease in the methane flux, as the sulphate profile is slightly concave down (Hensen et al., 2003). A decreasing methane flux is consistent with a setting where the supply of methane from hydrate dissociation drops as the hydrate reservoir declines.

Pore water sulphate profiles from the two deeper sites, where hydrate is expected to be stable year-round, are both kinked (PC01 and GC02; Fig. 5). In GC02 and the lower portion of PC01 the sulphate profiles are slightly concave up, which points to an increase in methane supply (Hensen et al., 2003; Nöthen and Kasten, 2011). This either implies that the methane flux at these sites has changed – consistent with thinning of the GHSZ near its landward limit (e.g., Marín-Moreno et al., 2015), or that the sediments have been affected by a mass deposition event (e.g., Hensen et al., 2003; Henkel et al., 2011). However, there are no obvious changes in sediment properties at the depth of the kink in the sulphate profile in these cores

Table 5
Methane fluxes across the sediment–seawater interface, and methane consumption by anaerobic oxidation of methane beneath the seafloor for the region of gas bubble plumes at the limit of the GHSZ offshore Western Svalbard (360–415 m water depth). Methane flux from bubble plumes, bubble plume density, and spatial extent of bubble plumes are from Sahling et al. (2014). Rate of AOM at bubble plume sites is from Berndt et al. (2014).

	Flux per unit area [mmol m^{-2} yr^{-1}]		Spatial extent	Total flux [mol yr^{-1}]		References
	Minimum	Maximum		Minimum	Maximum	
Methane flux across the sediment–seawater interface						
Ebullition flux	1.1×10^4	1.3×10^4	3.72 km^2, containing 384 (min) to 534 (max) bubble plumes	4×10^6	5×10^7	Sahling et al. (2014)
Irrigation flux	10	70	1.5 km^2: 30 m radius around each plume	2×10^4	1×10^5	This study
Diffusive flux	0.004	0.009	~7 km^2: 300 m radius around the bubble plume region (3.72 km^2)	2	5	This study
Methane consumption by AOM						
Gas bubble plumes	–	2×10^5	~10 m^2: within 0.01 to 0.1 m of plumes	30	4×10^4	Berndt et al. (2014)
Irrigation zone	300	600	1.5 km^2: 30 m radius around each plume	5×10^5	8×10^5	This study
Diffusive zone	30	100	~5.5 km^2: diffusive zone, excluding inner irrigation zone	5×10^4	2×10^5	This study
Regional background	–	20	80 km^2: area sampled in this study	–	2×10^6	This study

(Supplemental Figs. 7 and 8) that would be expected to accompany a mass deposition event.

Recent increases in the supply of methane to the shallow sediments are also consistent with the pore water data in core PC04, which was recovered within the seasonal hydrate stability zone defined by Berndt et al. (2014). While the pore water sulphate profile is well described by both the steady-state diffusion only and TR models, the results of the two disagree (Table 4). Furthermore, methane concentrations are very high (>1 mM) in the near-surface sulphate-containing (>20 mM) pore waters, which could indicate that AOM is unable to keep up with a recent increase in methane supply. More than 50 years are likely required for the microbial AOM community to respond to significant increases in sediment methane fluxes (Dale et al., 2008b).

The shape of the pore water $\delta^{13}C$-CH_4 profile at site PC04 is distinctly different from the other cores in which the SMTZ was sampled (Fig. 3): there is a small, negative (from ~−56 to −60‰) shift in $\delta^{13}C$-CH_4 at the base of the SMTZ (where SO_4^{2-} concentrations begin to increase towards the sediment surface), and a large positive shift (from ~−60 to −22‰) at the top of the SMTZ. In all other cores extremely low $\delta^{13}C$-CH_4 values are observed throughout the SMTZ (−97 to −83‰). During AOM, kinetics favour the oxidation of ^{12}C-CH_4, producing ^{13}C-depleted carbonate and a residual methane pool that is ^{13}C-enriched (e.g., Whiticar, 1999), as observed at the top of the SMTZ in PC04 ($\delta^{13}C$-CH_4 values up to −22‰; Fig. 3). However, low $\delta^{13}C$-CH_4 values measured at the depth of the SMTZ (i.e., ^{12}C rather than ^{13}C enriched, as in e.g. PC02, Fig. 3), are often observed and attributed to carbon cycling: AOM immediately above the SMTZ progressively enriches the local carbonate pool in ^{12}C which is recycled to methane with additional ^{12}C enrichment by methanogenesis occurring immediately below the SMTZ (Borowski et al., 1997). Alternatively, if the supply of sulphate from overlying seawater is very limited, enzyme-mediated equilibrium carbon isotope exchange can occur, producing a ^{12}C-enriched methane pool without coupled methanogenesis (Yoshinaga et al., 2014). These processes are summarized in Fig. 7.

Thus, according to Yoshinaga et al. (2014), if the supply of methane increases the SMTZ moves towards the seafloor and oxidation of methane occurs in the presence of high sulphate, resulting in ^{13}C-enriched residual methane. Conversely, a stable or decreasing methane supply leads to diffusion controlled methane oxidation and results in ^{12}C-enriched residual methane. For core PC04, the $\delta^{13}C$-CH_4 data are consistent with the occurrence of AOM in the presence of high sulphate and thus support the inference that the methane flux has recently increased. The absence of strongly ^{13}C-depleted methane beneath the SMTZ in core PC04 is also consistent with a recently increased methane flux that prevents the development of a well-established interval of carbon cycling at the SMTZ, in contrast to the other sites where stable methane fluxes have allowed a strongly ^{13}C-enriched carbon pool to accumulate over this sediment depth interval. Both processes may be occurring simultaneously, and both support the idea that methane fluxes have recently increased at this site.

It is clear that the supply of methane to shallow sediments in the vicinity of the LLGHSZ is largely unaffected by release of gas from hydrate. Geophysical surveys

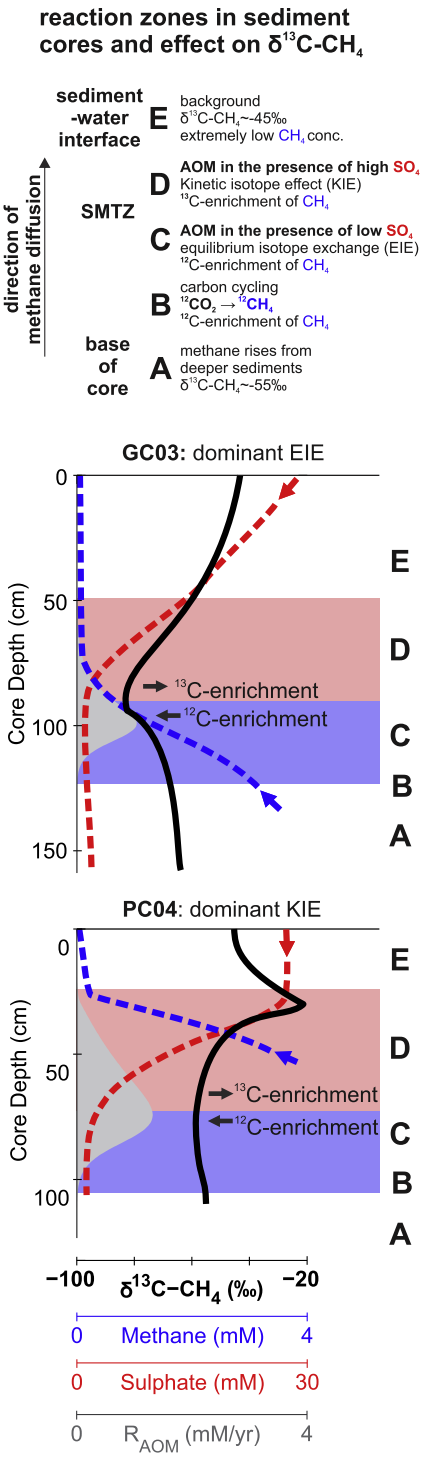

Fig. 7. Schematic illustration of the processes driving shifts in $\delta^{13}C\text{-}CH_4$ near the SMTZ. The interval in which AOM occurs (grey shaded area, modelled AOM rate as shown in Fig. 3), is divided into two zones: the upper area (pink, zone D) where AOM occurs in the presence of high sulphate concentrations favouring kinetic isotope fractionation, and the lower area in which AOM occurs in the presence of low sulphate concentrations favouring enzyme-mediated equilibrium isotope exchange (blue, zone C). (For interpretation of the references to colour in this figure legend, the reader is referred to the web version of this article.)

indicate that focused subsurface methane fluxes lead to small pockets of hydrate formation (e.g., Thatcher et al., 2013). Thus, a potential explanation for the absence of evidence for gas hydrate destabilization in this study is that the sampled sites missed locations where hydrate had been present. While the evidence for changes in subsurface methane supply that we observe in cores PC01, GC02 and PC04 is consistent with hydrate dissociation, alternative explanations including other processes that act to alter fluid flow pathways are also possible. These can only be properly evaluated if the coring density is significantly higher. Unfortunately, the glaciogenic nature of the uppermost sediments makes coring extremely difficult, so this will be hard to achieve.

5.3. AOM control on methane release from shallow sediments

The distinctive result from the modelling is that the fluxes of dissolved methane into the shallow subsurface sediments vary by an order of magnitude in cores taken close to (within ~0.01 to 0.3 km) the seafloor bubble plumes (30–550 mmol CH_4 m^{-2} yr^{-1}; Table 4). This is interpreted as the result of focusing of gases in cracks and small fractures in the low-permeability glaciogenic sediments (e.g., Thatcher et al., 2013). Dissolved methane fluxes into shallow subsurface sediments located at greater distance (~1 to 2.6 km) from the bubble plumes are slightly lower (10–20 mmol m^{-2} yr^{-1}; Table 4), but it is clear that methane pervades sediments across the entire West Svalbard continental margin. At most sites sampled in this study, only a tiny fraction of the methane delivered to the subsurface sediments is transferred across the seafloor by molecular diffusion: <0.01 mmol m^{-2} yr^{-1}.

Irrigation of the upper ~30 cm of sediment provides a mechanism for increasing the dissolved methane flux into bottom waters. Mixing of near-surface pore water with bottom seawater at methane seeps can be enhanced by bioirrigation by chemosynthetic organisms (Boudreau, 1997), and by the passage of bubble steams (Haeckel et al., 2007). Transport-reaction model results for PC04, where high methane concentrations are observed closest to the seafloor, yield an irrigation flux of 70 mmol CH_4 m^2 yr^{-1} into the overlying water column. Nevertheless, pore waters in sediment cores taken by submersible directly on top of active gas bubble plumes in our study area have much higher methane concentrations (up to 11 mM; Berndt et al., 2014), and the gas bubble (ebullition) flux of methane across the sediment–seawater interface is far higher (~1.1–13 × 10^3 mmol CH_4 m^{-2} yr^{-1}; Sahling et al., 2014; Table 5) than fluxes of methane delivered to the water column by diffusion or irrigation.

Our model results indicate that diffusive fluxes of methane across the sediment–seawater interface persist up to at least 300 m away from bubble plumes, whereas irrigation fluxes are likely restricted to within ~30 m of plumes. The spatial distribution of our sediment cores and modelled methane fluxes inform a rough estimate of the methane budget for the western Svalbard region (Table 5). Although the area of the seafloor affected by seepage of methane via diffusion is far greater than the area of seafloor affected by

seepage via irrigation or bubble ebullition, the total amount of methane emitted to the water column by ebullition (4×10^6 to 5×10^7 mol yr^{-1}; Table 5) is far greater than that emitted via irrigation (2×10^4 to 1×10^5 mol yr^{-1}; Table 5) or diffusion (2 to 5 mol yr^{-1}; Table 5). Fluxes of methane delivered to the water column by diffusion or irrigation are slightly lower than those estimated for the Håkon Mosby mud volcano located in the Barents Sea to the south ($\sim 6 \times 10^6$ mol yr^{-1}; Milkov et al., 2004). The total methane flux density (ebullition + irrigation + diffusion; 1.1–13.1 mol m^{-2} yr^{-1}, Table 5) is similar to that reported for methane ebullition on the East Siberian Arctic Shelf (0.2 to 14 mol m^{-2} yr^{-1}; Shakhova et al., 2014).

Model results reported in Table 5 indicate that >80% of the dissolved methane that enters the shallow subsurface sediments in the irrigation zone (within 30 m of seafloor bubble plumes), and >99.99% of the dissolved methane that enters the shallow subsurface sediments between 30 m and 300 m away from the bubble plumes is consumed by AOM. The rate of AOM is much higher at bubble plume sites (up to 11 μmol cm^{-3} day^{-1}; Berndt et al., 2014) than modelled in this study (<0.6 μmol cm^{-3} day^{-1}; Table 4; Fig. 5), but the proportion of methane oxidised is far lower (<0.1%; Table 5). Reduced AOM efficiency with increasing methane flux has been observed in other cold seep environments (e.g., Vanneste et al., 2011; Felden et al., 2013). Overall, we estimate that the proportion of all methane (dissolved + gas phase) entering the shallow subsurface sediments that is consumed by AOM amounts to ~10 % of the total flux to the shallow subsurface sediments. Localized high gas fluxes, likely resulting from the focusing of fluid flow through cracks within the relatively low permeability glaciogenic sediments (Thatcher et al., 2013), play a critical role in effecting the release of methane at the seafloor offshore western Svalbard.

6. SUMMARY AND CONCLUSIONS

The chemical compositions of gases in shallow sediments and bubble plumes and sediment pore water geochemistry provide no clear evidence for dissociation of hydrate close to the landward limit of the GHSZ offshore western Svalbard. Methane fluxes into shallow sediments appear to be at steady-state in all but one core (PC02). The chemical composition of the bubble plume gases is similar to that of a gas hydrate sample from a pockmark site ~30 km away from the LLGHSZ, suggesting that they may have the same gas source, but our data cannot distinguish between gas that has been released by dissociating hydrate and gas that has never been in the hydrate phase.

Pore waters from sediments within the seasonal GHSZ (PC04), and from deeper sites where hydrate is expected to be stable year-round (PC01 and GC02), provide some evidence for recent changes in the supply of methane from depth. This would be consistent with hydrate dissociation, or other processes which alter subsurface gas flow pathways. A higher sampling density is required to better constrain the cause of changes in methane supply to the LLGHSZ.

Our analyses show that methane pervades the shallow subsurface sediments offshore western Svalbard, but methane fluxes are highly spatially heterogeneous. If the methane flux to the shallow subsurface sediments is relatively low (30–120 mmol m^{-2} yr^{-1}), methane is largely consumed by anaerobic oxidation below the seabed, and the flux of methane across the seafloor is negligible. At higher methane fluxes (up to >~200 mmol m^{-2} yr^{-1}), irrigation of near-surface sediment pore waters increases transfer of methane into the water column (up to ~70 mmol m^{-2} yr^{-1}), but even this is insignificant compared to the quantity of methane transferred in the gas bubble plumes (up to ~16,000 mmol m^{-2} yr^{-1}; Sahling et al., 2014). Overall, AOM prevents less than 10% of the total methane delivered to shallow sub-surface sediments from reaching the overlying water column.

ACKNOWLEDGEMENTS

This project was funded by a UK Natural Environment Research Council (NERC) National Capability programme and NERC grant NE/D005728/2, and is part of a Ph.D. study funded by the Graduate School of Ocean and Earth Science (University of Southampton, UK) and Natural Sciences and Engineering Research Council of Canada Postgraduate Scholarships awarded to CAG (PGS-M and PGS-D3). The NERC Life Sciences Mass Spectrometry Steering Committee awarded a 'grant in kind' for $\delta^{13}C$-CH_4 analyses. We thank Captain M. Burgan of the RRS *James Clark Ross*, Captain K. Bergmann of the R/V *Maria S. Merian* and shipboard scientific parties, officers, and crews of cruises JCR 253 and MSM21/4. D. Green, B. Alker and C. Cole are thanked for their assistance with shipboard and shore-based chemical analyses, and K. Hissmann and J. Schauer for samples obtained with the JAGO submersible. All of the core material described in this paper is archived in BOSCORF at the National Oceanography Centre UK. We thank four anonymous reviewers, the Associate Editor, and Tim Minshull (University of Southampton) and Sandra Arndt (University of Bristol) for their constructive and insightful comments on an earlier version of this manuscript.

APPENDIX A. SUPPLEMENTARY DATA

Supplementary data associated with this article can be found, in the online version, at http://dx.doi.org/10.1016/j.gca.2016.11.015.

REFERENCES

Archer D. (2007) Methane hydrate stability and anthropogenic climate change. *Biogeosciences* **4**, 521–544.

Archer D., Buffett B. and Brovkin V. (2009) Ocean methane hydrates as a slow tipping point in the global carbon cycle. *Proc. Natl. Acad. Sci. U.S.A.* **106**, 20596–20601.

Berndt C., Feseker T., Treude T., Krastel S., Liebetrau V., Niemann H., Bertics V. J., Dumke I., Dünnbier K., Férre B., Graves C., Gross F., Hissmann K., Hühnerbach V., Krause S., Lieser K., Schauer J. and Steinle L. (2014) Temporal constraints on hydrate-controlled methane seepage off Svalbard. *Science* **343**, 284–287.

Boetius A., Ravenschlag K., Schubert C. J., Rickert D., Widdel F., Gieseke A., Amann R., Jørgensen B. B., Witte U. and Pfannkuche O. (2000) A marine microbial consortium apparently mediating anaerobic oxidation of methane. *Nature* **407**, 623–626.

Borowski W. S., Paull C. K. and Ussler W. (1996) Marine pore-water sulfate profiles indicate in situ methane flux from underlying gas hydrate. *Geology* **24**, 655–658.

Borowski W. S., Paull C. K. and Ussler W. (1997) Carbon cycling within the upper methanogenic zone of continental rise sediments: An example from the methane-rich sediments overlying the Blake Ridge gas hydrate deposits. *Mar. Chem.* **57**, 229–311.

Boudreau B. P. (1997) *Diagenetic Models and their Implementation: Modelling Transport and Reactions in Aquatic Sediments*. Springer Berlin, Heidelberg, NY.

Bowen G. J., Maibauer B. J., Kraus M. J., Röhl U., Westerhold T., Steimke A., Gingerich P. D., Wing S. L. and Clyde W. C. (2014) Two massive, rapid releases of carbon during the onset of the Palaeocene-Eocene thermal maximum. *Nat. Geosci.* **8**, 44–47.

Brass M. and Röckmann T. (2010) Continuous-flow isotope ratio mass spectrometry method for carbon and hydrogen isotope measurements on atmospheric methane. *Atmos. Meas. Tech.* **3**, 1707–1721.

Bünz S., Polyanov S., Vadakkepuliyambatta S., Consolaro C. and Mienert J. (2012) Active gas venting through hydrate-bearing sediments on the Vestnesa Ridge, offshore W-Svalbard. *Mar. Geol.* **332–334**, 189–197.

Carcione J. M., Gei D., Rossi G. and Madrussani G. (2005) Estimation of gas-hydrate concentration and free-gas saturation at the Norwegian-Svalbard continental margin. *Geophys. Prospect.* **53**, 803–810.

Ciais P., Sabine C., Bala G., Bopp L., Brovkin V., Canadell J., Chhabra A., DeFries R., Galloway J., Heimann M., Jones C., Le Quéré C., Myneni R. B., Piao S. and Thornton P. (2013) Carbon and other biogeochemical cycles. In *Climate Change 2013: The Physical Science Basis. Contribution of Working Group I to the Fifth Assessment Report of the Intergovernmental Panel on Climate Change* (eds. T. F. Stocker, D. Qin, G.-K. Plattner, M. Tignor, S. K. Allen, J. Boschung, A. Nauels, Y. Xia, V. Bex and P. M. Midgley). Cambridge University Press, Cambridge, UK, pp. 465–570.

Chabert A., Minshull T. A., Westbrook G. K., Berndt C., Thatcher K. E. and Sarkar S. (2011) Characterization of a stratigraphically constrained gas hydrate system along the western continental margin of Svalbard from ocean bottom seismometer data. *J. Geophys. Res.* **116**, B12102.

Claypool G. E., Threlkeld C. N., Mankiewicz P. N., Arthur M. A. and Anderson T. F. (1985) Isotopic composition of interstitial fluids and origin of methane in slope sediment of the Middle America trench, Deep-Sea Drilling Project Leg-84. *Init. Rep. Deep Sea Drilling Project* **84**, 683–691.

Dale A. W., Aguilera D. R., Regnier P., Fossing H., Knab N. J. and Jørgensen B. B. (2008) Seasonal dynamics of the depth and rate of anaerobic oxidation of methane in Aarhus Bay (Denmark) sediments. *J. Mar. Res.* **66**, 127–155.

Dale A. W., Van Cappellen P., Aguilera D. R. and Regnier P. (2008) Methane efflux from marine sediments in passive and active margins: Estimations from bioenergetic reaction–transport simulations. *Earth Planet. Sci. Lett.* **265**, 329–344.

Damm E., Mackensen A., Budéus G., Faber E. and Hanfland C. (2005) Pathways of methane in seawater: Plume spreading in an Arctic shelf environment (SW-Spitsbergen). *Cont. Shelf Res.* **25**, 1453–1472.

Dickens G. R. (2011) Down the rabbit hole: Toward appropriate discussion of methane release from gas hydrate systems during the Paleocene-Eocene thermal maximum and other past hyperthermal events. *Clim. Past* **7**, 831–846.

Dickens G. R. and Quinby-Hunt M. S. (1994) Methane hydrate stability in seawater. *Geophys. Res. Lett.* **21**, 2115–2118.

Dumke I., Burwicz E. B., Berndt C., Klaeschen D., Feseker T., Geissler W. H. and Sarkar S. (2016) Gas hydrate distribution and hydrocarbon maturation north of the Knipovich Ridge, western Svalbard margin. *J. Geophys. Res. Solid Earth* **121**, 1405–1424.

Egeberg P. K. and Dickens G. R. (1999) Thermodynamic and pore water halogen constraints on gas hydrate distribution at ODP Site 997 (Blake Ridge). *Chem. Geol.* **153**, 53–79.

Egger M., Rasigraf O., Sapart C. J., Jilbert T., Jetten M. S. M., Röckmann T., van der Veen C., Bândă N., Kartal B., Ettwig K. F. and Slomp C. P. (2015) Iron-mediated anaerobic oxidation of methane in brackish coastal sediments. *Environ. Sci. Technol.* **49**, 277–283.

Eiken O. and Hinz K. (1993) Contourites in the Fram Strait. *Sed. Geol.* **82**, 15–32.

Elverhøi A., Andersen E. S., Dokken T., Hebbeln D., Spielhagen R., Svendsen J. I., Sørflaten M., Rørnes A., Hald M. and Forsberg C. F. (1995) The growth and decay of the Late Weichselian ice sheet in western Svalbard and adjacent areas based on provenance studies of marine sediments. *Quat. Res.* **44**, 303–316.

Fehn U., Lu Z. and Tomaru H. (2006) Data report: ^{129}I/I ratios and halogen concentrations in pore water of hydrate ridge and their relevance for the origin of gas hydrates: a progress report. In *Proceedings of the Ocean Drilling Program Scientific Results*, Vol. 204 (eds. A. M. Trehu, G. Bohrmann, M. E. Torres and F. S. Colwell). Ocean Drilling Program, College Station, Texas.

Feisthauer S., Vogt C., Modrzynski J., Szlenkier M., Krüger M., Siegert M. and Richnow H. H. (2011) Different types of methane monooxygenases produce similar carbon and hydrogen isotope fractionation patterns during methane oxidation. *Geochim. Cosmochim. Acta* **75**, 1173–1184.

Felden J., Lichtschlag A., Wenzhöfer F., de Beer D., Feseker T., Ristova P. P., de Lange G. and Boetius A. (2013) Limitations of microbial hydrocarbon degradation at the Amon mud volcano (Nile deep-sea fan). *Biogeosciences* **10**, 3269–3283.

Ferré B., Mienert J. and Feseker T. (2012) Ocean temperature variability for the past 60 years on the Norwegian-Svalbard margin influences gas hydrate stability on human time scales. *J. Geophys. Res.* **117**, C10017.

Fisher R. E., Sriskantharajah S., Lowry D., Lanoisellé M., Fowler C. M. R., James R. H., Hermansen O., Lund Myhre C., Stohl A., Greinert J., Nisbet-Jones P. B. R., Mienert J. and Nisbet E. G. (2011) Arctic methane sources: Isotopic evidence for atmospheric inputs. *Geophys. Res. Lett.* **38**, L21803.

Forwick M., Baeten N. J. and Vorren T. O. (2009) Pockmarks in Spitsbergen fjords. *Norw. J. Geol.* **89**, 65–77.

Fuex A. N. (1980) Experimental evidence against an appreciable isotopic fractionation of methane during migration. In *Advances in Organic Geochemistry* (eds. E. M. Douglas and J. R. Maxwell). Pergamon, pp. 639–646.

Haeckel M., Boudreau B. P. and Wallmann K. (2007) Bubble-induced porewater mixing: A 3-D model for deep porewater irrigation. *Geochim. Cosmochim. Acta* **71**, 5135–5154.

Haeckel M., Suess E., Wallmann K. and Rickert D. (2004) Rising methane gas bubbles form massive hydrate layers at the seafloor. *Geochim. Cosmochim. Acta* **68**, 4335–4345.

Haese R. R., Meile C., Van Cappellen P. and De Lange G. J. (2003) Carbon geochemistry of cold seeps: Methane fluxes and transformation in sediments from Kazan mud volcano, eastern Mediterranean Sea. *Earth Planet. Sci. Lett.* **212**, 361–375.

Hautala S. L., Solomon E. A., Johnson H. P., Harris R. N. and Miller U. K. (2014) Dissociation of Cascadia margin gas hydrates in response to contemporary ocean warming. *Geophys. Res. Lett.* **41**, 8486–8494.

Hayduk W. and Laudie H. (1974) Prediction of diffusion coefficients for nonelectrolytes in dilute aqueous solutions. *AIChE J.* **20**, 611–615.

Henkel S., Strasser M., Schwenk T., Hanebuth T. J. J., Hüsener J., Arnold G. L., Winkelmann D., Formolo M., Tomasini J., Krastel S. and Kasten S. (2011) An interdisciplinary investigation of a recent submarine mass transport deposit at the continental margin off Uruguay. *Geochem. Geophys. Geosyst.* **12**, Q08009.

Hensen C., Zabel M., Pfeifer K., Schwenk T., Kasten S., Riedinger N., Schulz H. D. and Boetius A. (2003) Control of sulfate porewater profiles by sedimentary events and the significance of anaerobic oxidation of methane for the burial of sulfur in marine sediments. *Geochim. Cosmochim. Acta* **67**, 2631–2647.

Hester K. C. and Brewer P. G. (2009) Clathrate hydrates in nature. *Ann. Rev. Mar. Sci.* **1**, 303–327.

Hoehler T. M., Borowski W. S., Alperin M. J., Rodriguez N. M. and Paull C. K. (2000) Model, stable isotope, and radiotracer characterization of anaerobic methane oxidation in gas hydrate-bearing sediments of the Blake ridge. In *Proceedings of the Ocean Drilling Program, Scientific Results* (eds. C. K. Paull, R. Matsumoto, P. J. Wallace and W. P. Dillon). Ocean Drilling Program, College Station, Texas.

Hustoft S., Bünz S., Mienert J. and Chand S. (2009) Gas hydrate reservoir and active methane-venting province in sediments on 20 Ma young oceanic crust in the Fram Strait, offshore NW-Svalbard. *Earth Planet. Sci. Lett.* **284**, 12–24.

Jessen S. P., Rasmussen T. L., Nielsen T. and Solheim A. (2010) A new Late Weichselian and Holocene marine chronology for the western Svalbard slope 30,000–0 cal years BP. *Quat. Sci. Rev.* **29**, 1301–1312.

Johnson J. E., Mienert J., Plaza-Faverola A., Vadakkepuliyambatta S., Knies J., Bunz S., Andreassen K. and Ferré B. (2015) Abiotic methane from ultraslow-spreading ridges can charge Arctic gas hydrates. *Geology* **43**(5), 371–374.

Judd A. and Hovland M. (2007) *Seabed Fluid Flow: The Impact on Geology, Biology and the Marine Environment*. Cambridge University Press, Cambridge, UK.

Knies J., Damm E., Gutt J., Mann U. and Pinturier L. (2004) Near-surface hydrocarbon anomalies in shelf sediments off Spitsbergen: Evidences for past seepages. *Geochem. Geophys. Geosyst.* **5**, Q06003.

Knittel K. and Boetius A. (2009) Anaerobic oxidation of methane: Progress with an unknown process. *Annu. Rev. Microbiol.* **63**, 311–334.

Kretschmer K., Biastoch A., Rüpke L. and Burwicz E. (2015) Modeling the fate of methane hydrates under global warming. *Global Biogeochem. Cycles* **29**, 610–625.

Krey V., Canadell J. G., Nakicenovic N., Abe Y., Andruleit H., Archer D., Grubler A., Hamilton N. T. M., Johnson A., Kostov V., Lamarque J.-F., Langhorne N., Nisbet E. G., O'Neill B., Riahi K., Riedel M., Wang W. and Yakushev V. (2009) Gas hydrates: Entrance to a methane age or climate threat?. *Environ. Res. Lett.* **4** 034007.

Kvenvolden K. A. (1993) Gas hydrates: Geological perspective and global change. *Rev. Geophys.* **31**, 173–187.

Malinverno A. and Pohlman J. W. (2011) Modeling sulfate reduction in methane hydrate-bearing continental margin sediments: Does a sulfate-methane transition require anaerobic oxidation of methane? *Geochem. Geophys. Geosyst.* **12**, Q07006.

Marín-Moreno H., Minshull T. A., Westbrook G. K., Sinha B. and Sarkar S. (2013) The response of methane hydrate beneath the seabed offshore Svalbard to ocean warming during the next three centuries. *Geophys. Res. Lett.* **40**, 5159–5163.

Marín-Moreno H., Minshull T. A., Westbrook G. K. and Sinha B. (2015) Estimates of future warming-induced methane emissions from hydrate offshore west Svalbard for a range of climate models. *Geochem. Geophys. Geosyst.* **16**, GC005737.

Mazumdar A., Joäo H. M., Peketi A., Dewangan P., Kocherla M., Joshi R. K. and Ramprasad T. (2012) Geochemical and geological constraints on the composition of marine sediment pore fluid: Possible link to gas hydrate deposits. *Mar. Petrol. Geol.* **38**, 35–52.

Meister P., Liu B., Ferdelman T. G., Jørgensen B. B. and Khalili A. (2013) Control of sulphate and methane distributions in marine sediments by organic matter reactivity. *Geochim. Cosmochim. Acta* **104**, 183–193.

Milkov A. V. (2004) Global estimates of hydrate-bound gas in marine sediments: How much is really out there? *Earth Sci. Rev.* **66**, 183–197.

Milkov A. V. (2005) Molecular and stable isotope compositions of natural gas hydrates: A revised global dataset and basic interpretations in the context of geological settings. *Org. Geochem.* **36**, 681–702.

Milkov A. V., Claypool G. E., Lee Y.-J. and Sassen R. (2005) Gas hydrate systems at Hydrate Ridge offshore Oregon inferred from molecular and isotopic properties of hydrate-bound and void gases. *Geochim. Cosmochim. Acta* **69**, 1007–1026.

Milkov A. V., Vogt P. R., Crane K., Lein A. Y., Sassen R. and Cherkashev G. A. (2004) Geological, geochemical, and microbial processes at the hydrate-bearing Håkon Mosby mud volcano: A review. *Chem. Geol.* **205**, 347–366.

Möller L., Sowers T., Bock M., Spahni R., Behrens M., Schmitt J., Miller H. and Fischer H. (2013) Independent variations of CH_4 emissions and isotopic composition over the past 160,000 years. *Nat. Geosci.* **6**, 885–890.

Nauhaus K., Boetius A., Krüger M. and Widdel F. (2002) *In vitro* demonstration of anaerobic oxidation of methane coupled to sulphate reduction in sediment from a marine gas hydrate area. *Environ. Microbiol.* **4**, 296–305.

Nisbet E. G., Dlugokencky E. J. and Bousquet P. (2014) Methane on the rise—again. *Science* **343**, 493–495.

Nöthen K. and Kasten S. (2011) Reconstructing changes in seep activity by means of pore water and solid phase Sr/Ca and Mg/Ca ratios in pockmark sediments of the Northern Congo Fan. *Mar. Geol.* **287**, 1–13.

Nuzzo M., Hornibrook E. R. C., Gill F., Hensen C., Pancost R. D., Haeckel M., Reitz A., Scholz F., Magalhães V. H., Brückmann W. and Pinheiro L. M. (2009) Origin of light volatile hydrocarbon gases in mud volcano fluids, Gulf of Cadiz — Evidence for multiple sources and transport mechanisms in active sedimentary wedges. *Chem. Geol.* **266**, 350–363.

Panieri G., James R. H., Camerlenghi A., Westbrook G. K., Consolaro C., Cacho I., Cesari V. and Sanchez Cervera C. (2014) Record of methane emissions from the West Svalbard continental margin during the last 23,500 years revealed by d13C of benthic foraminifera. *Global Planet. Change* **122**, 151–160.

Pape T., Bahr A., Rethemeyer J., Kessler J. D., Sahling H., Hinrichs K.-U., Klapp S. A., Reeburgh W. S. and Bohrmann G. (2010) Molecular and isotopic partitioning of low-molecular-weight hydrocarbons during migration and gas hydrate precipitation in deposits of a high-flux seepage site. *Chem. Geol.* **269**, 350–363.

Parmentier F.-J. W., Christensen T. R., Sørensen L. L., Rysgaard S., McGuire A. D., Miller P. A. and Walker D. A. (2013) The impact of lower sea-ice extent on Arctic greenhouse-gas exchange. *Nat. Clim. Change* **3**, 195–202.

Piñero E., Marquardt M., Hensen C., Haeckel M. and Wallmann K. (2013) Estimation of the global inventory of methane hydrates in marine sediments using transfer functions. *Biogeosciences* **10**, 959–975.

Plaza-Faverola A., Bünz S., Johnson J. E., Chand S., Knies J., Mienert J. and Franek P. (2015) Role of tectonic stress in seepage evolution along the gas hydrate-charged Vestnesa Ridge, Fram Strait. *Geophys. Res. Lett.* **42**, 733–742.

Pohlman J. W., Kaneko M., Heuer V. B., Coffin R. B. and Whiticar M. (2009) Methane sources and production in the northern Cascadia margin gas hydrate system. *Earth Planet. Sci. Lett.* **287**, 504–512.

Pohlman J. W., Riedel M., Bauer J. E., Canuel E. A., Paull C. K., Lapham L., Grabowski K. S., Coffin R. B. and Spence G. D. (2013) Anaerobic methane oxidation in low-organic content methane seep sediments. *Geochim. Cosmochim. Acta* **108**, 184–201.

Prinzhofer A. and Pernaton E. (1997) Isotopically light methane in natural gas: Bacterial imprint or diffusive fractionation? *Chem. Geol.* **142**, 193–200.

Rajan A., Mienert J. and Bünz S. (2012) Acoustic evidence for a gas migration and release system in Arctic glaciated continental margins offshore NW-Svalbard. *Mar. Petrol. Geol.* **32**, 36–49.

Reagan M. T. and Moridi G. J. (2007) Oceanic gas hydrate instability and dissociation under climate change scenarios. *Geophys. Res. Lett.* **34**, L22709.

Reagan M. T. and Moridis G. J. (2009) Large-scale simulation of methane hydrate dissociation along the West Spitsbergen Margin. *Geophys. Res. Lett.* **36**, L23612.

Regnier P., Dale A. W., Arndt S., LaRowe D. E., Mogollón J. and Van Cappellen P. (2011) Quantitative analysis of anaerobic oxidation of methane (AOM) in marine sediments: A modeling perspective. *Earth Sci. Rev.* **106**(1–2), 105–130.

Roy S., Hovland M., Noormets R. and Olaussen S. (2015) Seepage in Isfjorden and its tributary fjords, West Spitsbergen. *Mar. Geol.* **363**, 146–159.

Sahling H., Römer M., Pape T., Bergès B., dos Santos Fereirra C., Boelmann J., Geprägs P., Tomczyk M., Nowald N., Dimmler W., Schroedter L., Glockzin M. and Bohrmann G. (2014) Gas emissions at the continental margin west of Svalbard: Mapping, sampling, and quantification. *Biogeosciences* **11**, 6029–6046.

Sapart C. J., van der Veen C., Vigano I., Brass M., van de Wal R. S. W., Bock M., Fischer H., Sowers T., Buizert C., Sperlich P., Blunier T., Behrens M., Schmitt J., Seth B. and Röckmann T. (2011) Simultaneous stable isotope analysis of methane and nitrous oxide on ice core samples. *Atmos. Meas. Tech.* **4**, 2607–2618.

Sarkar S., Berndt C., Chabert A., Masson D. G., Minshull T. A. and Westbrook G. K. (2011) Switching of a paleo-ice stream in northwest Svalbard. *Quat. Sci. Rev.* **30**, 1710–1725.

Sarkar S., Berndt C., Minshull T. A., Westbrook G. K., Klaeschen D., Masson D. G., Chabert A. and Thatcher K. E. (2012) Seismic evidence for shallow gas-escape features associated with a retreating gas hydrate zone offshore west Svalbard. *J. Geophys. Res.* **117**, B09102.

Schoell M. (1983) Genetic characterization of natural gases. *AAPG Bull.* **67**, 2225–2238.

Shakhova N., Semiletov I., Leifer I., Sergienko V., Salyuk A., Kosmach D., Chernykh D., Stubbs C., Nicolsky D., Tumskoy V. and Gustafsson Ö. (2014) Ebullition and storm-induced methane release from the East Siberian Arctic Shelf. *Nat. Geosci.* **7**, 64–70.

Skarke A., Ruppel C., Kodis M., Brothers D. and Lobecker E. (2014) Widespread methane leakage from the sea floor on the northern US Atlantic margin. *Nat. Geosci.* **7**, 657–661.

Sloan E. D. (1998) *Clathrate Hydrates of Natural Gases*, second ed. Marcel Dekker, New York, p. 705.

Smith A. J., Mienert J., Bünz S. and Greinert J. (2014) Thermogenic methane injection via bubble transport into the upper Arctic Ocean from the hydrate-charged Vestnesa Ridge, Svalbard. *Geochem. Geophys. Geosyst.* **15**, 1945–1959.

Spielhagen R. F., Werner K., Sørensen S. A., Zamelczyk K., Kandiano E., Budeus G., Husum K., Marchitto T. M. and Hald M. (2011) Enhanced modern heat transfer to the Arctic by warm Atlantic Water. *Science* **331**, 450–453.

Sun X. and Turchyn A. V. (2014) Significant contribution of authigenic carbonate to marine carbon burial. *Nat. Geosci.* **7**, 201–204.

Thatcher K. E., Westbrook G. K., Sarkar S. and Minshull T. A. (2013) Methane release from warming-induced hydrate dissociation in the West Svalbard continental margin: Timing, rates, and geological controls. *J. Geophys. Res. Solid Earth* **118**, 22–38.

Tréhu A. M., Long P. E., Torres M. E., Bohrmann G., Rack F. R., Collett T. S., Goldberg D. S., Milkov A. V., Riedel M. and Schultheiss P. (2004) Three-dimensional distribution of gas hydrate beneath southern Hydrate Ridge: constraints from ODP Leg 204. *Earth Planet. Sci. Lett.* **222**, 845–862.

Treude T., Boetius A., Knittel K., Wallmann K. and Jørgensen B. B. (2003) Anaerobic oxidation of methane above gas hydrates at Hydrate Ridge, NE Pacific Ocean. *Mar. Ecol. Prog. Ser.* **264**, 1–14.

Vanneste H. (2010) *Seepage of Hydrocarbon Bearing Fluids at the Carlos Riberiro and Darwin Mud Volcanoes (Gulf of Cardiz)* (Ph. D. thesis). Univ. of Southampton.

Vanneste H., Kelly-Gerreyn B. A., Connelly D. P., James R. H., Haeckel M., Fisher R. E., Heeschen K. and Mills R. A. (2011) Spatial variation in fluid flow and geochemical fluxes across the sediment–seawater interface at the Carlos Ribeiro mud volcano (Gulf of Cadiz). *Geochim. Cosmochim. Acta* **75**, 1124–1144.

Vanneste M., Guidard S. and Mienert J. (2005) Bottom-simulating reflections and geothermal gradients across the western Svalbard margin to the Molloy Transform Fault. *Terra Nova* **17**, 510–516.

Vogt P. R., Gardner J. and Crane K. (1999) The Norwegian-Barents-Svalbard (NBS) continental margin: Introducing a natural laboratory of mass wasting, hydrates, and ascent of sediment, pore water, and methane. *Geo. Mar. Lett.* **19**, 2–21.

Wallmann K., Pinero E., Burwicz E., Haeckel M., Hensen C., Dale A. and Ruepke L. (2012) The global inventory of methane hydrate in marine sediments: a theoretical approach. *Energies* **5**, 2449–2498.

Wang D. T., Gruen D. S., Lollar B. S., Hinrichs K. U., Stewart L. C., Holden J. F., Hristov A. N., Pohlman J. W., Morrill P. L., Könneke M., Delwiche K. B., Reeves E. P., Sutcliffe C. N., Ritter D. J., Seewald J. S., McIntosh J. C., Hemond H. F., Kubo M. D., Cardace D., Hoehler T. M. and Ono S. (2015) Nonequilibrium clumped isotope signals in microbial methane. *Science* **348**(6233), 428–431.

Westbrook G. K., Thatcher K. E., Rohling E. J., Piotrowski A. M., Pälike H., Osborne A. H., Nisbet E. G., Minshull T. A., Lanoisellé M., James R. H., Hühnerbach V., Green D., Fisher R. E., Crocker A. J., Chabert A., Bolton C., Beszczynska-Möller A., Berndt C. and Aquilina A. (2009) Escape of methane gas from the seabed along the West Spitsbergen continental margin. *Geophys. Res. Lett.* **36**, L15608.

Whiticar M. J. (1999) Carbon and hydrogen isotope systematics of bacterial formation and oxidation of methane. *Chem. Geol.* **161**, 291–314.

Yoshinaga M. Y., Holler T., Goldhammer T., Wegener G., Pohlman J. W., Brunner B., Kuypers M. M. M., Hinrichs K.-U. and Elvert M. (2014) Carbon isotope equilibration during sulphate-limited anaerobic oxidation of methane. *Nat. Geosci.* **7**, 190–194.

Zhang T. and Krooss B. M. (2001) Experimental investigation on the carbon isotope fractionation of methane during gas migration by diffusion through sedimentary rocks at elevated temperature and pressure. *Geochim. Cosmochim. Acta* **65**, 2723–2742.

Associate editor: Thomas Wagner